Palaeobiology of latest Ediacaran phosphorites from the upper Khesen Formation, Khuvsgul Group, northern Mongolia

Palaeobiology of latest Ediacaran phosphorites from the upper Khesen Formation, Khuvsgul Group, northern Mongolia

Ross P. Anderson[1,2,3*], Sean McMahon[1,4], Francis A. Macdonald[5], David S. Jones[6], and Derek E.G. Briggs[1,7]

[1]Department of Geology and Geophysics, Yale University, 210 Whitney Avenue, New Haven, CT, 06511, USA

[2]All Souls College, University of Oxford, Oxford, OX1 4AL, UK

[3]Department of Earth Sciences, University of Oxford, South Parks Road, Oxford, OX1 3AN, UK

[4]UK Centre for Astrobiology, School of Physics and Astronomy, University of Edinburgh, James Clerk Maxwell Building, Peter Guthrie Tait Road, Edinburgh, EH9 3FD, UK

[5]Department of Earth and Planetary Sciences, Harvard University, 20 Oxford Street, Cambridge, MA, 02138, USA

[6]Geology Department, Amherst College, 11 Barrett Hill Road, Amherst, MA, 01002, USA

[7]Peabody Museum of Natural History, Yale University, 170 Whitney Avenue, New Haven, CT, 06511, USA

*Corresponding Author

Email: ross.anderson@all-souls.ox.ac.uk

Telephone: (+44) 01865 281 404

Abstract

Microfossil assemblages that include large acritarchs with complex processes, known as Doushantuo-Pertatataka-type acritarchs, are recovered from early-Ediacaran successions globally. They are commonly found in shale and chert lithologies, but their diversity and palaeobiological significance is greatest when they are phosphatized. The best-known example is from the Doushantuo Formation, South China, which preserves over 60 taxa including possible embryonic forms which may represent the oldest fossil animals. Fossils have only been recorded in four Ediacaran phosphorite deposits. Here we report the fifth such occurrence, from phosphorites of the upper Khesen Formation, Khuvsgul Group, northern Mongolia, where preservation rivals that in the Doushantuo Formation. The assemblage includes the likely cyanobacteria *Obruchevella delicata*, *O. magna*, *O. parvissima*, and *O. valdaica*, as well as various *Siphonophycus* filaments, the possible alga *Archaeophycus yunnanensis*, and the Doushantuo-Pertatataka-type acritarchs *Appendisphaera grandis*, *A. fragilis*, *A. tenuis*, *Cavaspina basiconica*, *Variomargosphaeridium gracile* and *V. aculeiparvum*, sp. nov.. The phosphorites also preserve the multicellular embryo-like taxon *Megasphaera*, which is represented by *M. minuscula* sp. nov. and potentially by *M. puncticulosa*. Geological and chemostratigraphic data suggest a latest Ediacaran age for the Khesen assemblage, immediately prior to the Proterozoic–Phanerozoic boundary. Thus, this is the youngest Doushantuo-Pertatataka-type microfossil assemblage yet described. It extends the range of *Appendisphaera*, *Cavaspina*, *Megasphaera*, and *Variomargosphaeridium* upward by tens of millions of years. The assemblage adds to a growing database of Ediacaran fossils and emphasizes the importance of Mongolian strata to understanding the transition from a broadly microbial Proterozoic Eon to a Phanerozoic Eon where macroscopic animals acted as geobiological agents.

Keywords

Acanthomorphic acritarchs; fossilized embryos; Ediacaran; phosphatized microfossils; Mongolian fossils; Doushantuo Lagerstätte

Introduction

Three-dimensional phosphatized microfossils from the Doushantuo Formation of South China have provided critical information on Ediacaran communities (e.g., Xiao *et al.* 2014a). The Doushantuo Formation, particularly where it is exposed at Weng'an, yields the highest diversity of eukaryotic fossils known from the first ~4 billion years of Earth history (Liu *et al.* 2014; Xiao *et al.* 2014b; Cohen & Macdonald 2015). Dominant are large (commonly >100 μm) acanthomorphic acritarchs (Doushantuo-Pertatataka-type) which offer a potential biostratigraphic framework for Ediacaran successions (Xiao *et al.* 2016): similar fossils are known from shales and early diagenetic cherts in Australia (Grey 2005; Willman *et al.* 2006; Willman 2007; Willman & Moczydłowska 2008, 2011), eastern Europe (Vorob'eva *et al.* 2009a; Golubkova *et al.* 2015), India (Shukla & Tiwari 2014; Joshi & Tiwari 2016), Siberia (Moczydłowska *et al.* 1993; Sergeev *et al.* 2011; Moczydłowska & Nagovitsin 2012), and Svalbard (Knoll 1992). Some of the fossils show early examples of multicellularity and they may represent animal embryos or resting cysts (Xiao *et al.* 1998; Xiao & Knoll 2000; Hagadorn *et al.* 2006; Yin *et al.* 2007; Chen *et al.* 2009b; Cohen *et al.* 2009; Yin *et al.* 2013; Chen *et al.* 2014; Xiao *et al.* 2014a), in which case the Doushantuo fossils are the oldest body fossils of animals known from the geological record. However, their phylogenetic affinities are controversial and a recent study concluded that none of the characters used to argue a

metazoan affinity are confined to animals (Cunningham *et al.* 2017). These multicellular forms have otherwise been interpreted as sulphur-oxidizing bacteria (Bailey *et al.* 2007), unicellular protists (Bengtson *et al.* 2012), mesomycetozoean-like holozoans (Huldtgren *et al.* 2011), and *Volvox*-like green algae (Xue *et al.* 1995; Butterfield 2011). The Doushantuo Formation has also yielded representatives of florideophyte red algae (Xiao *et al.* 2004), and perhaps even sponge-grade fossils (Yin *et al.* 2015).

Despite the importance of Lagerstätten to studies of Ediacaran diversity and the transition to an Earth with animals as geobiological agents, few are known from the phosphorite deposits that represent this interval (Cook & Shergold 1986; Muscente *et al.* 2017). Phosphatized fossils have recently been reported from the Denying Formation in China, although they may represent reworked clasts from the underlying Doushantuo Formation (Zhang & Zhang 2017). The Biskopås Formation, Norway has yielded a variety of Doushantuo-Pertatataka-type acanthomorphic acritarchs but multicellular taxa have not been recovered (Spjeldnaes 1963, 1967; Vidal 1990). The Chambaghat Formation in India has yielded possible analogs for Doushantuo fossils although the material discovered to date is not as well-preserved (Shome *et al.* 2014).

Mongolia preserves a diverse Neoproterozoic–early Palaeozoic sedimentary record (Macdonald *et al.* 2009; Macdonald 2011; Macdonald & Jones 2011; Johnston *et al.* 2012; Bold *et al.* 2013; Bold *et al.* 2016a; Bold *et al.* 2016b; Smith *et al.* 2016), which has yielded a variety of fossils (e.g., Bosak *et al.* 2011a; Bosak *et al.* 2011b; Cohen *et al.* 2015; Anderson *et al.* 2017b). The Khuvsgul terrane of northern Mongolia, in particular, hosts economic-grade phosphorite deposits (Donov *et al.* 1967; Ilyin 1973; Ilyin *et al.* 1986; Osokin & Tyzhinov 1998; Ilyin 2004; Macdonald & Jones 2011). The high preservation potential of organic microfossils in phosphorites makes Mongolia an obvious target for new Lagerstätten, which might inform the debate about the phylogenetic affinities of these early organisms.

Here we present the systematic palaeontology of the recently discovered Khesen Lagerstätte (Anderson *et al.* 2017a), which includes Doushantuo-Pertatataka-type acanthomorphs and other microfossils, including animal embryo-like forms, and discuss its biostratigraphic and palaeobiologic significance.

Geological setting

The fossils reported here are from phosphorites of the Khesen Formation of the Khuvsgul Group (Figs. 1 and 2). The formation is discontinuously exposed on the Khuvsgul terrane over 250 km along the western margin of Lake Khuvsgul in north Mongolia (Macdonald & Jones 2011). The stratigraphy of this terrane shares a symmetry with that of the Zavkhan terrane in southwest Mongolia (Figs. 2A–B) as both formed a continuous margin during Neoproterozoic–Cambrian time (Macdonald *et al.* 2009; Kuzmichev & Larionov 2011; Macdonald 2011; Macdonald & Jones 2011; Bold *et al.* 2016a; Bold *et al.* 2016b; Smith *et al.* 2016). Both successions are characterized by (1) ~800 Ma arc-volcanic rocks overlain by (2) late Tonian rift-related strata, (3) Cryogenian–early Ediacaran carbonate platforms that incorporate records of two Snowball Earth glaciations (the ~717–655 Ma Sturtian glaciation and the ~640–635 Ma Marinoan glaciation), and (4) latest Ediacaran to early Cambrian foreland basin successions, which preserve the fossils reported here. The foreland successions, which host the latest Ediacaran-Terreneuvian phosphorites, formed on both terranes as a result of the collision of the Khantaishir-Agradag arc (Bold *et al.* 2016a; Smith *et al.* 2016).

One of the most striking features of the stratigraphy of the Zavkhan terrane is an unconformity in the foreland succession that separates early Ediacaran carbonates of the Ol and Shuurgat formations from latest Ediacaran phosphorites and carbonates of the terminal

Ediacaran Zuun-Arts Formation (Bold *et al.* 2016b; Smith *et al.* 2016). An equivalent unconformity is present in the Khesen Formation on the Khuvsgul terrane. This unconformity divides the formation into informal lower and upper members (Fig. 2). It separates a carbonate succession of early Ediacaran age from latest Ediacaran to early Cambrian carbonate, shale, and fossiliferous phosphorite deposits (Donov *et al.* 1967; Ilyin 1973; Ilyin *et al.* 1986; Osokin & Tyzhinov 1998; Macdonald & Jones 2011). A minimum age constraint for the upper Khesen Formation is provided by early Cambrian archaeocyathids and trilobites in the overlying Erkhelnur Formation (Ilyin & Zhuraveleva 1968; Korobov 1980).

The Khesen Formation generally thins to the north (Figs. 2C–E). This is due in part to the unconformity, manifested in stratigraphic truncations below the phosphorite interval, which places it directly above Marinoan age glacial deposits of the lower Khesen Formation (Macdonald & Jones 2011). Near Ongoluk Gol, more than 50 m of carbonate-dominated strata separate the glacial deposits from the phosphorite (Fig. 2C). Lateral correlations are further complicated by faulting within the Khesen Formation, particularly at Khesen Gol, poor exposure in the recessive phosphorite interval, and lateral facies changes. In the Khesen syncline, the Khesen phosphorites consist broadly of an upper and lower unit, which are separated by a distinctive black chert bed (Ilyin *et al.* 1986). The lower phosphorite unit is further separated into upper and lower phosphate beds (Fig. 2), and the fossils described here are from the lower bed of Ilyin *et al.* (1986). However, it must be emphasized that these are mainly early diagenetic and reworked phosphorites distributed over several meters of stratigraphy, and showing large lateral facies changes, rather than discrete beds. Thus, they may not be robust stratigraphic markers throughout the basin but all likely formed during the latest Ediacaran–earliest Cambrian.

The two most diverse samples, YPM 536747, M618 32.0 and YPM 536748, M618 33.0, derive from granular phosphorites in the M618 succession (Fig. 1B) along the ridgeline

east of Urandush Uul (at 21 and 22 m in Fig. 2E). Here the Khesen Formation consists predominantly of thinly bedded grey dolomite interbedded with granular and laminated phosphorite deposits (Fig. 2E). The grains are sub-rounded to sub-angular and range in size from medium to coarse sand (Fig. 3). Fossils are preserved within these grains or form grains themselves, and may have been transported after phosphatization. Many of the Doushantuo-Pertatataka-type fossils in the Doushantuo Formation, South China, are found in similar facies (e.g., Dornbos *et al.* 2006; Muscente *et al.* 2015) and sometimes occur as bioclastic grains (Xiao & Knoll 2000).

Materials and methods

Forty-eight rock samples were investigated from 11 stratigraphic suites (M602, M603, M605, M609, M610, M611, M612, M615, M617, M618, M619), derived from four main localities, Khirbisteg Gol, Ongoluk Gol, Khesen Gol, and along the ridgeline east of Urandush Uul (Fig. 1).

Rock samples, thin-sections, and scanning electron microscopy (SEM) stubs are deposited in the collections of the Yale Peabody Museum of Natural History (YPM) Division of Invertebrate Paleontology. Each sample, thin-section, and figured microfossil or population (e.g., in the case of the filamentous fossil *Siphonophycus* many specimens are shown in the same illustration) is given a YPM collection number. Unique sample identifications are given for samples and thin-sections (e.g., M618 32.0 A). We follow the International Code of Nomenclature for Algae, Fungi, and Plants.

Petrographic thin-sections 30 μm-thick were cut sub-perpendicular to bedding. Only a single section was prepared from each of the rock samples except the two that were most fossiliferous. Four thin-sections (YPM 536728, M618 32.0 A; YPM 536729, M618 32.0 B;

YPM 536730, M618 32.0 C; YPM 536731, M618 32.0 D) were cut from YPM 536747, M618 32.0 and eight (YPM 536732, M618 33.0 A; YPM 536733, M618 33.0 B; YPM 536734, M618 33.0 C; YPM 536735, M618 33.0 D; YPM 536736, M618 33.0 E; YPM 536737, M618 33.0 F; YPM 536738, M618 33.0 G; YPM 536739, M618 33.0 H) from YPM 536748, M618 33.0. A Jenopik CF scan camera on a Leica DM 2500 P petrographic microscope was used to prepare photomicrographs. The camera combines multiple high magnification pictures to produce high resolution images. Maximum dimensions of fossil vesicles were measured on all examples encountered in thin-section. Dimensions of cellular processes were also measured.

Small <2 cm^3 sub-samples of YPM 536747, M618 32.0 and YPM 536748, M618 33.0 were macerated in 20% acetic acid for 48–72 hours, dissolving the carbonate matrix and releasing phosphatized microfossils. The insoluble residue, which included the fossils, was washed in deionized water and dried at 40 °C. Fossils were hand-picked under a Leica MZ16 stereo microscope, and mounted on aluminium stubs for examination via SEM. The success of this maceration technique was variable; partially silicified samples, especially YPM 536748, M618 33.0, typically resisted fossil extraction by this method, confining investigation to thin-sections. Similar issues have been reported for certain samples from the Doushantuo Formation in South China (e.g., Xiao *et al.* 2014b). Fossils isolated by maceration were imaged uncoated using gaseous secondary electrons on a FEI/Philips XL-30 environmental scanning electron microscope operating at 10 kV.

A number of samples in the Khesen Formation yielded phosphatized microfossils (8 genera and up to 18 species). Not all fossil taxa were encountered in both thin-section and acid maceration. All taxa except *Obruchevella delicata* are represented in the two most diverse samples: YPM 536747, M618 32.0 and YPM 536748, M618 33.0. Five genera and 12 species are unique to these two samples (Table 1). Two samples from Khesen Gol, YPM

536746, M602 176.0 and YPM 536749, M602 179.0, also yielded an array of fossils (0 and 3 m in Fig. 2D) including the only examples of *O. delicata* but only a single acanthomorphic acritarch specimen. Several other samples from M602, M603, M611, M612, M615, and M619 yielded isolated filaments or spheres that may represent fossils, although the content of vesicles is commonly opaque and/or shrunken suggesting degradation (e.g., Golubic & Barghoorn 1977; Raff *et al.* 2006) and a time lag between death and phosphatization.

Systematic palaeontology

Oscillatoriacean Cyanobacteria

Genus ***Obruchevella*** Reitlinger, 1948, emend. Yakschin & Luchinina, 1981; Kolosov, 1984, Yankauskas, 1989; Burzin, 1995; Nagovitsin, 2000

Type species. *Obruchevella delicata* Reitlinger, 1948.

Obruchevella delicata Reitlinger, 1948

(Fig. 4A)

For synonymy see Schopf *et al.* (2015).

Material. Rare fossils (n = <10) in thin-section YPM 536696, M602 176.0 B.

Remarks. Regular tubes coiled into cylindrical spirals are assigned to the common Ediacaran–Cambrian fossil *Obruchevella delicata*. The maximum external diameter of the spirals is ~40 μm and their total length is ~150 μm; the diameter of the tubes is ~12 μm. We note the similarity of these specimens of *O. delicata* to *Obruchevella parva* (Reitlinger 1959; Golovenok & Belova 1989; Burzin 1995). The distinguishing characters of the two taxa have become confused through many emendations, so we follow Sergeev *et al.* (2012) and use the original descriptions (Reitlinger 1948, 1959; Golovenok & Belova, 1989) and diagnostic

dimensions as a basis for identifying these fossils as *O. delicata* (tube diameter = 10–13 μm; spiral outer diameter = 36–50 μm).

Obruchevella magna Golovenok & Belova, 1989

(Figs. 4B–D)

1992 *Obruchevella magna*, Knoll, p. 757, pl. 1, figs. 1, 3, and 5.

2010 *Obruchevella magna*, Golubkova *et al.*, p. 364, pl. 2, fig. 13.

Material. Two specimens (in thin-sections YPM 536731, M618 32.0 D and YPM 536732, M618 33.0 A) and an acid extracted specimen from YPM536747, M618 32.0.

Remarks. Large tubes in tight spirals are assigned to *Obruchevella magna*. The length of the spiral varies from 140–235 μm with a maximum outer diameter of 160–200 μm. The maximum diameter of the tube is 36–50 μm (all measurements from thin-sections). The spiral may taper towards one end, but this may be an artefact of thin-sectioning at an oblique angle to the specimen (both spiral diameter and tube diameter decrease to the lower left in Fig. 4B). Figure 4C shows that the spirals do not come into contact with each other, but this may be a result of the preservation of this specimen as an internal mould. Figure 4D shows a transverse cross section through *O. magna*. One of the specimens occurs in intimate association with *O. valdaica* (the specimens illustrated in Figs. 4B and G are next to each other).

Obruchevella parvissima Song, 1984

(Figs. 4E–F)

For synonymy see Schopf *et al.* (2015).

Material. Rare (n = <10) fossils in thin-section YPM 536734, M618 33.0 C.

Remarks. Thin-walled regular tubes coiled into loose spirals are assigned to *Obruchevella parvissima*. The external diameter of the spirals is 20–30 μm and the diameter of the tubes is ~5 μm. The fossil commonly appears significantly degraded (e.g., farthest right in Fig. 4F).

Obruchevella valdaica (Asseyeva, 1974) Jankauskas *et al.*, 1989

(Fig. 4G)

For synonymy see Sharma and Shukla (2012)

Material. A single specimen in thin-section YPM 536732, M618 33.0 A.

Remarks. A long (>400 μm) spiral comprising at least 23 tight revolutions with external spiral diameter of 90 μm is assigned to *Obruchevella valdaica*. The tubes are oval in cross section and ~12 μm in maximum diameter, with their short axis parallel to the long axis of the spiral. While the diameter of the tubes is within the diagnostic range of *O. delicata*, the spiral diameter is much larger than reported occurrences (the outer spiral diameter of *O. delicata* can reach up to 50 μm: Sergeev *et al.*, 2012). *O. valdaica* has an outer diameter between 46 and 270 μm (Sergeev *et al.*, 2012). The cell wall of each tube in our specimen is distinct, but there is a concentration of dark organic matter surrounding it. The fossil is found in intimate association with *O. magna*. The length of the spiral is greater than is commonly found (Sergeev *et al.*, 2012). However shorter spirals could be fragments of larger ones and length is not a good criterion for taxonomic identification.

?Algae

Genus ***Archaeophycus*** Wang *et al.*, 1983, emend. Dong *et al.*, 2009

Type species. *Archaeophycus venutus* Wang *et al.*, 1983.

Archaeophycus yunnanensis Song in Luo *et al.*, 1982

(Figs. 5A–E)

For synonymy see Dong *et al.* (2009).

Material. Clusters in thin-section YPM 536731, M618 32.0D and an acid-extracted specimen from sample YPM 536747, M618 32.0.

Remarks. Cells, either solitary or evident as dyad, triad, tetrad, and octad clusters (Figs. 5A–F), are assigned to *Archaeophycus yunnanensis*. The cells are 6–18 μm in diameter (mean = 11.4 μm, standard deviation = 1.1 μm, n = 45, all measurements from thin-sections) with dark cell walls (<2 μm thick). T-shaped cell division is evident in the acid-extracted specimen YPM 538070 (Fig. 5F). Although the size range of individual cells from the Khesen Formation is slightly larger than those from Ediacaran and Cambrian successions in China, which range from 9-15 μm (Dong *et al.* 2009), we do not consider this difference sufficient to warrant the erection of a new species. Furthermore, degradation has resulted in some redistribution of organic matter in the cell wall resulting in a "smudged" appearance in thin-section (Figs. 5A–E) which may account for slight variations in size. Clusters reach up to 32 μm in maximum dimension in thin-section, and the extracted specimen is 180 μm across.

The tetrad form (Fig. 5D) of the fossil was previously compared (as *Paratetraphycus giganteus*) to carposporangia of *Porphyra*, a modern bangialean alga (Xiao *et al.* 1998; Yoon *et al.* 2006; Dong *et al.* 2009; Adl *et al.* 2012). Xiao *et al.* (2014a), however, noted the morphological simplicity of the tetrad cell packets, and argued that convergent evolution among cyanobacteria, red algae, and green algae could not be ruled out. The phylogenetic affinity of this taxon remains elusive.

Acritarchs

Genus ***Appendisphaera*** Moczydłowska *et al.*, 1993, emend. Moczydłowska, 2005

Type species. *Appendisphaera grandis* Moczydłowska *et al.*, 1993, emend. Moczydłowska, 2005.

Appendisphaera grandis Moczydłowska *et al.*, 1993, emend. Moczydłowska, 2005

(Figs. 6A–D)

For synonymy see Xiao *et al.* (2014b).

Material. A single specimen from thin-section YPM 536731, M618 32.0 D.

Remarks. A vesicle (Figs. 6A–D) of maximum dimension 86 μm with numerous, densely-spaced long, thin, hollow processes, 16–28 μm in length and ~1 μm in maximum diameter is assigned to *Appendisphaera grandis*. The vesicle is within the described range of this species, but its processes are slightly longer as a proportion of this dimension (33% versus the previously described maximum of 25%) (Moczydłowska *et al.* 1993; Moczydłowska 2005). The hollow nature of many of the processes in this specimen is obscured due to their slender nature and the redistribution of organic matter during degradation (e.g., Figs. 6C–D). A similar phenomenon was reported in this species by Moczydłowska (2005).

An area of dense, dark organic matter is present between the processes (Figs. 6C–D). Moczydłowska *et al.* (1993) tentatively considered processes that coalesce to form a membrane-like structure as diagnostic of the species *A. tabifica* from the Siberian Platform. Specimens with similar but shorter coalesced processes were subsequently reported from Australia as *A. barbata* (Grey 2005). *A. tabifica* and *A. barbata* were regarded as potentially conspecific by Willman & Moczydłowska (2008). In contrast to the processes in these Siberian and Australian forms, some of those of the Khesen fossil extend beyond the darker rim (Figs. 6B–D). Zhang *et al.* (1998) argued that the darker area in the Siberian specimens may be a taphonomic artefact, possibly reflecting organic matter trapped between the densely spaced processes (see Moczydłowska *et al.* 1993). We consider this likely in the case of the Khesen specimen and assign it to *A. grandis* rather than *A. tabifica* or *A. barbata*, which may represent taphonomic variants (Zhang *et al.* 1998; Liu *et al.* 2014).

A. grandis was reported from Doushantuo phosphorites in South China by (Xiao *et al.* 2014b) based on a single specimen. They noted that the processes on this specimen were spaced slightly further apart than in examples from the Siberian type locality (Moczydłowska

et al. 1993; Moczydłowska 2005). They attributed this discrepancy to taphonomic and observational factors (i.e., comparing a specimen in thin-section from phosphorite with one extracted from shale with the processes compressed onto one another). The spacing of the processes in the Khesen specimen resembles that in the Doushantuo example (cf. Xiao *et al.* (2014b)) supporting its assignment to *A. grandis*.

Appendisphaera fragilis Moczydłowska *et al.*, 1993, emend. Moczydłowska, 2005

(Figs. 6E–G)

For synonymy see Moczydłowska (2005).

Material. Two specimens in thin-section YPM 536732, M618 33.0 A and one from thin-section YPM 536697, M602 179.0 A.

Remarks. Vesicles with maximum diameters 64–98 μm and numerous densely-spaced hollow processes (8–16 μm in length, <1 μm in maximum diameter, <2 μm between processes) are assigned to *Appendisphaera fragilis*. The length of processes is 13–24% of the maximum vesicle dimension, which is slightly greater than the range diagnostic for *A. fragilis* (Moczydłowska, 2005). This difference likely reflects a contrast in preservation and observation, comparing a Khesen specimen in thin-section with compressed acid-extracted Siberian specimens (Moczydłowska *et al.* 1993; Moczydłowska, 2005). Processes are cylindrical and flexible (Figs. 6E–G). They may converge giving the appearance of larger tapering processes (Fig. 6F). The hollow nature of the processes may be obscured, as in *A. grandis,* due to the redistribution of organic matter during degradation. An area of darker material between the processes in the Khesen specimen extends approximately two thirds of their length from the vesicle rim (Figs. 6E, G) and probably represents trapped organic matter that is taphonomic/diagenetic in origin. A number of the vesicles are infilled with silica, presumably during diagenesis.

Appendisphaera tenuis Moczydłowska *et al.*, 1993, emend. Moczydłowska, 2005

(Figs. 6F–I)

For synonymy see Xiao *et al.* (2014b).

Material. A single specimen in thin-section YPM 536730, M618 32.0 C.

Remarks. A specimen (Figs. 6H–I) with vesicle 112 μm in maximum diameter, circular in outline and presumably originally spherical, is assigned to *Appendisphaera tenuis* based on its size and process architecture. The processes are short (4–8 μm, ~7% of vesicle diameter), thin (<2 μm in maximum diameter), and cylindrical (Fig. 6I). They are slightly shorter relative to the vesicle diameter than those of *A. tenuis* (Moczydłowska (2005). However, Xiao *et al.* (2014b) reported specimens of *A. tenuis* with processes <7% of vesicle diameter. The processes in the Khesen specimen appear to expand slightly at their base, in a similar fashion to examples illustrated by Moczydłowska (2005), although the quality of preservation makes this feature difficult to confirm (Fig. 6I). Moczydłowska (2005) regarded the processes of *A. tenuis* as hollow. The evidence indicates that the processes in the single Khesen specimen are hollow although the walls may appear to merge distally (Fig. 6F).

Genus ***Cavaspina*** Moczydłowska *et al.*, 1993

Type species. *Cavaspina acuminata* (Kolosova, 1991) Moczydłowska *et al.*, 1993.

Cavaspina basiconica Moczydłowska *et al.*, 1993

(Figs. 7A–F)

For synonymy see Xiao *et al.* (2014b).

Material. 18 acid-extracted specimens from YPM 536747, M618 32.0.

Remarks. Specimens identified in acid residues with conical processes that taper acutely distally are assigned to *Cavaspina*. Three species have been described in addition to the type: *C. amplitudinis* Willman & Moczydłowska (2011); *C. basiconica* Moczydłowska *et al.* (1993); and *C. uria* Moczydłowska & Nagovitsin (2012) and Nagovitsin *et al.* (2004) and the

complex taxonomic history of the genus has been reviewed (Moczydłowska 2005; Moczydłowska *et al.* 1993). The Khesen material is assigned to *C. basiconica* based on the density and morphology of the processes.

The vesicles are spherical, 140–307 μm in maximum diameter (mean = 185.5 μm, standard deviation = 42.1 μm, n = 18), and usually compressed (Fig. 7F) so that they appear oblate. The maximum length of the processes is 3–38 μm (mean = 10.7 μm, standard deviation = 7.3 μm, n = 18), which is 2–13% (mean = 5.5 %, standard deviation is 2.3%, n = 18) of the maximum diameter of the vesicle that bears them. Processes taper distally from a maximum basal width of 16 μm (mean = 6.4, standard deviation = 2.8, range = 3–16, n = 18).

The vesicles are larger and commonly bear longer processes than the type material of *C. basiconica* from Siberia (Moczydłowska *et al.* 1993), but the specimens are closely similar morphologically to examples tentatively identified as *C. basiconica* from the Doushantuo Formation (Xiao *et al.* 2014b figs. 8.1–8.4) These Doushantuo specimens, which reach a dimension of up to 508 μm, were previously identified as *Meghystrichosphaeridium chadianensis* (Zhang *et al.* 1998; Zhou *et al.* 2001; Moczydłowska 2005; Xiao *et al.* 2014b). The processes in *Cavaspina* are usually <10 % of the maximum vesicle diameter. All 18 Khesen specimens fall within this threshold except YPM 538072 (Fig. 7A) which has processes that reach 13 %. We include this specimen in the same taxon but note that it could represent *Tanarium* which has similar but longer processes (typically >20 % of maximum vesicle diameter) (Moczydłowska *et al.* 1993; Grey 2005; Moczydłowska 2005).

One of the Khesen specimens (Fig. 7D) reveals large interior oblate structures which might represent internal cells, but we consider a diagenetic origin more likely. Some of the specimens display small holes in the vesicle ~10 μm in maximum dimension (Fig. 7B). Similar holes in Tonian vase-shaped microfossils of the Chuar Group might be the work of predatory protists (Porter, 2011; 2016). In the case of the Khesen fossils, however, they may

be the result of the loss of a process that communicated with the vesicle interior. In one specimen, the vesicle has ruptured (Fig. 7E) and wrinkled suggesting that the vesicle wall was pliable (Fig. 7F).

Genus ***Leiosphaeridia*** Eisenack, 1958, emend. Downie & Sarjeant, 1963; Turner, 1984

Type species. *Leiosphaeridia baltica* Eisenack, 1958.

Remarks. Simple organic walled vesicles are often assigned to the form genus *Leiosphaeridia*, which includes many described species (Jankauskas *et al.*, 1989). We follow Butterfield *et al.* (1994) in recognizing species differentiated by size and wall thickness. Leiospheres are more ubiquitous than other forms within the Khesen phosphorites and are present in the four samples (YPM 536747, M618 32.0, YPM 536748, M618 33.0, and YPM 536746, M602 176.0, YPM 536749, M602 179.0) that yielded the bulk of Khesen diversity. They may also be represented by poorly defined spherical structures in other samples.

The Khesen leiospheres are commonly infilled with silica (Figs. 8F, I, K) and are sometimes surrounded by a diagenetic halo (Fig. 8M).

Leiosphaeridia crassa (Naumova, 1949) Jankauskas, 1989

(Figs. 8A–E)

For synonymy see Butterfield *et al.* (1994) and Porter & Riedman (2016).

Materials. A single population (n = 37) is identified in thin-section YPM 536731, M618 32.0 D.

Remarks. Simple spherical fossils < 70 μm in maximum dimension (Figs. 8A–E) are assigned to *Leiosphaeridia crassa*. The cells are arranged close together with cell walls occasionally in contact (Figs. 8A–B). The cluster is ~200 μm by 600 μm in dimension. Individual cells range from 24 to 40 μm in maximum dimension (mean = 34.6 μm, standard deviation = 3.8 μm, n = 37: Fig. 8N).

L. crassa is differentiated from *L. minutissima* (Naumova 1949; Jankauskas *et al.* 1989) by the thickness of its cell wall—a character that may depend on taphonomy (Butterfield *et al.* 1994). Butterfield *et al.* (1994) used the degree to which the cell wall appears translucent in extracted shale-hosted specimens as an estimate of its likely thickness. Such comparisons are difficult to make based on thin-sections. The population of *Leiosphaeridia* identified in the Khusvgul phosphorites, however, preserves definitive cell walls which may exceed 1 μm in thickness (e.g., some of the specimens in Fig. 8B), so we place them in *L. crassa* but note that they may represent specimens of *L. minutissima*.

While the cells are commonly translucent, the interior may be darker and even opaque (e.g., Figs. 8C–E). This colouration presumably reflects degradation of the organic matter within the cell. Occasionally, interiors contain more regular structures (e.g., Fig 8D), which may be real rather than an artefact of degradation.

Leiosphaeridia jacutica (Timofeev, 1966) Mikhailova & Jankauskas, 1989

(Figs. 8F–K)

For synonymy see Butterfield *et al.* (1994) and Porter & Riedman (2016).

Material. Specimens are common in thin-sections of samples YPM 536746, M602 176.0, YPM 536749, M602 179.0, YPM 536747, M618 32.0 and YPM 536748, M618 33.0, with possible examples in thin-sections from samples YPM 536827, M611 91.0, YPM 536825 M611 93.8, and YPM 536820, M615 42.0.

Remarks. Thick-walled single-celled vesicles >70 μm are assigned to *Leiosphaeridia jacutica*. Specimens range in size from 88 to 360 μm (mean = 166.4 μm, standard deviation = 57.4 μm, n = 31: Fig. 8N). The broad size distribution and lack of diagnostic characters suggests that specimens assigned to *L. jacutica* may represent a variety of biological species (e.g., Butterfield *et al.* 1994).

The main distinction between *L. jacutica* and *L. tenuissima* (below) is its much thicker cell wall. Khesen specimens identified as *L. jacutica* commonly have a dark thick wall (Figs. 8F–K). Degradation may lead to redistribution of organic matter prior to fossilization resulting in artificial thickening of the cell wall (Fig. 8K appears to show a double wall that is likely a product of diagenesis), obscuring the distinction between *L. jacutica* and *L. tenuissima*. Due to the degraded nature of the wall in many specimens we do not provide statistical data on its thickness but note that it is ~5 μm.

The fossils assigned to *L. jacutica* commonly preserve interior structure. One specimen (Figs. 8G–H) accommodates an abundance of small subspherical features up to 3 μm in diameter. More commonly irregular dark areas are present (Figs. 8I–J) which may be a result of shrinkage and disaggregation during degradation.

Leiosphaeridia tenuissima Eisenack, 1958

(Figs. 8L–M, 10I)

For synonymy see Liu *et al.* (2014) and Porter & Riedman (2016).

Materials. Specimens commonly occur in thin-sections of samples from YPM 536746, M602 176.0, YPM 536749, M602 179.0, YPM 536747, M618 32.0 and YPM536748, M618 33, with possible examples in thin-sections from samples in M611 and M615.

Remarks. Thin-walled (<1 μm) vesicles >70 μm in maximum dimension are identified as *Leiosphaeridia tenuissima*. Khesen specimens range from 56 to 620 μm in maximum dimension (mean = 153.6 μm, standard deviation = 85.3 μm, n = 54: Fig. 8N). The size distribution is skewed left toward values <170 μm; there is only one specimen >310 μm.

The size distributions of *L. tenuissima* and *L. jacutica* are similar: in both cases over 80% of specimens are <200 μm in maximum dimension. However, 59% of specimens of *L. tenuissima* are <140 μm compared to 35% of *L. jacutica*. Butterfield *et al.* (1994) argued that

the overlap in size distribution casts doubt on the separation of the two species but we retain them here based on the difference in the thickness of the cell walls.

Specimens of *L. tenuissima*, like those of *L. jacutica*, commonly show internal structures (Fig. 8L) which are probably a result of shrinkage and disaggregation during decay. Furthermore, the entire vesicle of *L. tenuissima* can be opaque.

***Leiosphaeridia* spp.**

Remarks. The specimens of *Leiosphaeridia* from the Khesen phosphorites show a greater diversity than is revealed simply by size and wall thickness. The internal structures in different species are probably taphonomic, as is the halo on some specimens, but they may conceal biological differences. We therefore follow Butterfield *et al.* (1994) in listing *Leiosphaeridia* spp. to acknowledge that other species may be present.

Genus ***Megasphaera*** Chen & Liu, 1986, emend. Xiao & Knoll, 2000; Xiao *et al.*, 2014

Type species. *Megasphaera inornata* Chen & Liu, 1986, emend. Xiao *et al.*, 2014.

Remarks. Xiao *et al.* (2014b) defined the iconic animal embryo-like *Megasphaera* as large spherical vesicles, smooth or sculptured externally but without processes, accommodating one or more cells. Xiao & Knoll (2000) confined *Megasphaera* to vesicles enclosing a single cell, whereas the genera *Parapandorina* and *Megaclonophycus* accommodated 2–100 and >100 cells respectively (Xiao & Knoll, 2000). Xiao *et al.* (2014b) recognized these as developmental stages of *Megasphaera* and emended the diagnosis of the genus based on an interpretation of the sequence of cell division (Yuan *et al.* 2002; Zhou *et al.* 2002; Chen 2004; Yin *et al.* 2004; Xiao *et al.* 2007; Chen *et al.* 2009a; Xiao *et al.* 2012). They differentiated species of *Megasphaera* based on vesicle sculpture.

Prior to this discovery (Anderson *et al.* 2017a) *Megasphaera* had only been reported from the Doushantuo and Denying Formations, South China (Xiao *et al.* 2014b; Zhang &

Zhang 2017), and the Chambaghat Formation, India (Shome *et al.* 2014) and there has been a vigorous debate about its nature and affinities. It was initially interpreted as a metazoan embryo— the oldest body fossil evidence of metazoans in the geological record (Xiao *et al.* 1998). Subsequent authors interpreted *Megasphaera* as a sulphur-oxidizing bacterium (Bailey *et al.* 2007), unicellular protist (Bengtson *et al.* 2012), mesomycetozoean-like holozoan (Huldtgren *et al.* 2011), or *Volvox*-like green alga (Xue *et al.* 1995; Butterfield 2011), while others adhered to its interpretation as a metazoan or even bilaterian embryo (Xiao *et al.* 1998; Xiao & Knoll 2000; Hagadorn *et al.* 2006; Yin *et al.* 2007; Chen *et al.* 2009b; Cohen *et al.* 2009; Yin *et al.* 2013). This last interpretation was extended to argue an affinity with different multicellular eukaryotes, such as stem-group animals and algae, based on patterns of cell differentiation (Chen *et al.* 2014; Xiao *et al.* 2014a). Chen et al. (2014) also provided evidence against the bacterial, unicellular protist, mesomycetozoean-like holozoan, and volvox hypotheses. Despite these advances it remains the case that none of the characters currently available are unequivocally diagnostic of an animal affinity (Cunningham *et al.* 2017).

Anderson *et al.* (2017b) described a fossil from the early Ediacaran Shuurgat Formation, Mongolia, which, in spite of being degraded, showed similarities to *Megasphaera* (Anderson *et al.* 2017b, figs. 9H, I). Here we describe a new species from Khesen phosphorites—the second confirmed example outside South China.

Megasphaera minuscula sp. nov.

(Figs. 9A–M, 10A–H, 10J–K, 11A–J)

Holotype. YPM 536784 (Figs. 9C–D).

Diagnosis. Medium-sized (50–400 μm maximum diameter) smooth-walled vesicle. One or more cells may be enclosed within the vesicle.

Derivation of name. Latin *minuscula* meaning smaller.

Material. 48 specimens in thin-sections of samples YPM 536747, M618 32.0 and YPM 536748, M618 33.0; several acid-extracted specimens from YPM 536747, M618 32.0.

Occurrence. Ediacaran, Khesen Formation, Khuvsgul Group, northern Mongolia.

Description. Specimens are medium sized spheroidal vesicles with no processes, enclosing internal cellular structures. The vesicles are 76–325 μm in maximum dimension (mean = 135.7 μm, standard deviation = 35.9 μm, n = 48: Fig. 9N) and usually circular, suggesting an originally spherical shape—some have suffered minor compaction resulting in a more oval outline. Specimens enclose cellular structures that are circular, oval, or irregular (degraded) in outline. There is large variability in the preservation of the cellular structures (Figs. 9–11). The cell margins are well-preserved in only six of the 48 fossils (Figs. 9A–M), and the cells are rarely in contact, presumably due to degradation and shrinkage. The cells are normally poorly-preserved and appear as "ghosts" without clear boundaries (Figs. 10A–K). The overall vesicle diameter appears unaffected by degradation, however, as the size distributions of those with well-preserved as opposed to poorly-preserved cells overlap (Fig. 9N): well-preserved: mean = 144.7 μm, standard deviation = 28.0 μm, n = 6, range = 96–172 μm; poorly-preserved: mean = 134.4 μm, standard deviation = 37.0 μm, n = 42, range = 76–325 μm (the largest specimen is an outlier at 325 μm). The maximum dimension of individual cellular structures within the six well-preserved specimens ranges from 3 to 26 μm (mean = 10.5 μm, standard deviation = 5.2 μm, n = 282). It is difficult to estimate the maximum number of cellular structures and their size range in thin section due to indifferent preservation. Counts ranged from 20 to 106 per vesicle (YPM 536784, Figs. 9C–D shows fewer than YPM 536766, Figs. 9J–K), but it is clear that not all cellular structures are evident. The mean dimension of cellular structures in the well-preserved specimens ranges from 5.1 to 16.6 μm. The standard deviation within an individual vesicle is never more than 29% of the mean (range = 4–29%) suggesting that the internal structures are relatively uniform in size.

The mean size of the internal bodies increases as a function of vesicle diameter ($R^2 = 0.7407$: Fig. 10L). Some features probably represent taphonomic artefacts. In some specimens, for example, the outer envelope has been lost and the cellular structures appear as a cluster of poorly outlined small bodies (Figs. 10G–H; the remains of the wall are evident above the cluster in Fig 10G). In other specimens, the vesicle walls are thickened by diagenetic phosphate; YPM 536761 appears to show low projections on the outer wall (Fig. 10J) but it is unclear whether or not these are artefacts of diagenetic mineralization. The structures within YPM 536811 appear to be covered by a granular orange mineral (Fig. 10E)..

Specimens released by acid maceration fall within the same vesicle size range as those observed in thin-section (< 400 μm). The vesicle wall is smooth. It is difficult to determine whether these specimens represent *Megasphaera* or are similar leiospheres unless they are broken to reveal the interior (specimens illustrated in Figs. 11A–B may represent either leiospheres or *Megasphaera*). Phosphatic features may form within leiospheres during diagenesis and might be confused with cellular structures (Figs. 11F–I). In some cases, phosphatic filaments, which may be fossilized bacteria (Xiao & Knoll 1999), cover the interior of the specimens (Fig. 11H). Alternatively, the filaments may represent phosphatic infilling of the voids between internal cells that subsequently degraded. Similar structures are common in Doushantuo examples (cf. Xiao & Knoll 1999, fig.7; Chen *et al.* 2014, fig. 3B). Yin *et al.* (2014) reported a number of poorly-preserved embryo-like fossils similar to some of our acid-extracted specimens. Despite these difficulties some of our Khesen specimens clearly show internal cells (Figs. 11C–E). YPM 538073 (Fig. 11E) appears to contain a shrunken body which occupies only a proportion of the vesicle interior. It may represent a shrunken single cell or the shrunken mass of degraded material within the vesicle, and resembles a specimen illustrated by Xiao and Knoll (2000, Fig. 3.7). YPM 538718 and YPM 538074 (Figs. 11C–D) retain fragments of the vesicle wall enclosing internal bodies; the wall

thickness (~8 μm thick) is commensurate with that of *Megasphaera inornata* (Xiao & Knoll, 2000; Xiao *et al.*, 2014b). In contrast, the wall of YPM 538719 (Fig. 11H) is much thinner. YPM 538721 has a raised equatorial area (Fig. 11I) but its ovoid shape suggests that this may be the result of compression at the poles and creasing of the envelope, likely a result of deflation.

Remarks. *Megasphaera minuscula* is erected to accommodate specimens that differ from other *Megasphaera* species in their smaller external vesicle size. Previously described *Megasphaera* species are at least 200 μm in maximum diameter, and unornamented species more than 400 μm (Xiao *et al.* 2014b). *M. minuscula* is unornamented, but does not exceed 400 μm.

The size distribution of *M. minuscula* overlaps that of Khesen specimens of *Leiosphaeridia tenuissima*. The only character separating these taxa is the presence of internal cellular bodies in *Megasphaera*, and when this character is obscured via decay and/or diagenesis they are difficult to distinguish (cf. fig. 3 in Xiao & Knoll 2000).

Other fossils smaller (50–150 μm) than previously described *Megasphaera* that likewise contain internal cellular bodies were described from early diagenetic chert nodules of the Doushantuo Formation (cf. fig. 117 parts 6, 7, and 18 in Liu *et al.* 2014). They designated these fossils as "leiospheres with cellular inclusions" rather than as a species of *Megasphaera* noting that they likely represent ontogenetic stages of multiple taxa and are similar in size to *L. tenuissima*. Liu *et al.* (2014) also noted the similarity between their Doushantuo leiospheres and large species of *Clonophycus* from early diagenetic chert nodules of Cambrian China (Taozichong formations) (Luo *et al.* 1982). Vesicles of *Clonophycus* range from 8–90 μm (Oehler 1977, 1978): the higher part of this range is represented by the Chinese species *C. guizhouensis* (42–90 μm in maximum dimension, internal cells of maximum diameter 10–25 μm) (Luo *et al.* 1982). In contrast to the

Doushantuo "leiospheres with cellular inclusions" and to *Clonophycus guizhouensis*, the Khesen fossils are preserved in phosphorite in a similar manner to *Megasphaera* (Xiao *et al.* 2014b). A number of Khesen specimens are intermediate in size between leiospheres with cellular inclusions and *Clonophycus* on the one hand, and the smallest specimens of *M. inornata* on the other. The Khesen specimens preserve a taphonomic sequence in which the internal cellular inclusions shrink and decay prior to the outer vesicle itself (Fig. 10). Thus, we assign this Khesen form to a new species of *Megasphaera* since it is readily accommodated by the emended diagnosis of the genus (Xiao *et al.* 2014b). Some of the fossils described by Liu *et al.* (2014) as "leiospheres with cellular inclusions" and by Luo *et al.* (1982) as *Clonophycus*, may represent *M. minuscula*.

One of the best preserved Khusvgul specimens (YPM 536766, Figs. 9J–K) contains an unusually large number of internal structures in a vesicle that falls on the smaller end of the size range of *Megasphaera minuscula* (Fig. 9N). Xiao *et al.* (2014b) noted that the number of internal structures is dependent on ontogenetic stage and therefore not a good criterion for distinguishing taxa—the cells decrease in size and increase in number while the dimensions of the outer envelope remain the same.

One of the specimens may hint at greater diversity within *Megasphaera* in the Khesen Formation. YPM 538797 (Fig. 11J), 540 μm in maximum dimension, bears a stalk-like feature (~100 μm in length, ~75 μm in maximum diameter at base), which is reminiscent of the funiculus on a lobster egg (cf. fig. 1a in Martin *et al.* 2003 and in Martin *et al.* 2004). Such egg stalks function to attach the eggs to the pleopods (appendages) of the adult crustacean, or to each other. If this Khesen structure were a funiculus it would be consistent with interpretations of the envelope of *Megasphaera* as a diapause egg cyst (e.g., Yin *et al.* 2007) or envelope containing an embryo. The fossil resembles *Ceratosphaeridium* from the Officer Basin in Australia (Grey 2005) in the possession of a single large process. The

Khesen specimen is much larger, however, (540 μm compared to 50–160 μm) with a more robust process (those on *Ceratosphaeridium* are 20–50 μm in length and do not exceed 15 μm in diameter). The same specimen (YPM 538797) also has an oval shaped "crater" on its surface (~40 μm in maximum dimension, see arrow in Fig. 11J). Such "craters" have previously been described (see p. 773 in Xiao & Knoll 2000) although they occur on the internal body and not the outer envelope. Xiao & Knoll (2000) argued that such craters were preservational artefacts, but they might represent the insertion of similar stalk-like bodies. The crater on the Khesen specimen, however, is considerably smaller than the diameter of the stalk and likely represents an artefact of preservation.

Megasphaera ?puncticulosa Xiao et al. 2014b

(Fig. 11K–L)

Material. A single acid extracted specimen YPM 538720 from YPM 536747, M618 32.0

Remarks. The external surface of this specimen (almost 400 μm in maximum dimension, Figs. 11J–K) is covered in circular elevated structures each <5 μm in maximum diameter and separated by < 5 μm and may represent a different species of *Megasphaera*. We tentatively assign it to *Megasphaera puncticulosa*. In the type material illustrated by Xiao et al. (2014b) the bumps are commonly preserved as holes that presumably penetrate the entire thickness of the vesicle wall. A specimen (cf. fig. 24.2 and 24.3 in Xiao et al., 2014b), however, preserves these features as small elevated structures, as in the Khesen specimen.

Genus ***Variomargosphaeridium*** Zang in Zang & Walter, 1992, emend. Xiao *et al.*, 2014

Type species. *Variomargosphaeridium litoschum* Zang in Zang & Walter, 1992.

Remarks. The most abundant Doushantuo-Pertatataka-type acanthomoprhic acritarch identified in the Khesen phosphorites is assigned to *Variomargosphaeridium gracile* based on the morphology of its branching processes. Xiao *et al.* (2014b) noted that *Alicesphaeridium,*

Ancorosphaeridium, Archaeotunisphaeridium, Densisphaera, Dicrospinosphaera, Multifronsphaeridium, Tanarium, and *Variomargosphaeridium* all include at least some species with branching processes. *Alicesphaeridium* species with branching processes always bear some that are unbranched (Zang & Walter 1992; Grey 2005; Willman & Moczydłowska 2008; Vorob'eva *et al.* 2009b). *Ancorosphaeridium* is characterized by processes with anchor-like terminations (Sergeev *et al.* 2011; Moczydłowska & Nagovitsin,2012). The processes in *Archaeotunisphaeridium* are thin and cylindrical with distal filaments and fimbriae (Grey 2005). The processses in *Densisphaera* support an outer membrane and have no connection with the vesicle interior (Moczydłowska & Nagovitsin 2012). Xiao *et al.* (2014b) emended the diagnosis of *Variomargosphaeridium* to include processes that are heteromorphic, hollow, cylindrical or basally widened, and multi-branched, and which communicate with the vesicle interior. Branching can be successive or terminal, commonly forming a crown. The processes of *Dicrospinosphaera* are much thinner, reportedly solid, and branch less profusely than those of *Variomargosphaeridium* (Yuan & Hofmann 1998). *Multifronsphaeridium* is characterized by fewer and larger processes than *Variomargosphaeridium*; the vesicle is reported to be planoconvex (Zang & Walter 1992; Grey 2005). Xiao *et al.* (2014b) raised the possibility of synonymizing *Multifronsphaeridium* with *Variomargosphaeridium* as its vesicle shape may be diagenetic in origin. Branched processes also occur in a few species of *Tanarium* but very rarely (Moczydłowska *et al.* 1993; Grey 2005; Moczydłowska 2005; Willman & Moczydłowska 2011).

Variomargosphaeridium gracile Xiao *et al.*, 2014

(Figs. 12A–O, 13A–F)

For synonymy see Xiao *et al.* (2014b).

Material. Sixty specimens in thin-sections from Khesen samples YPM 536747, M618 32.0 and YPM 536748, M618 33.0.

Remarks. Xiao *et al.* (2014b) distinguished the species *V. gracile* based on its small vesicle size (30–150 μm in maximum diameter) and thin processes (9–21 μm in length). Khesen vesicles that range from 92 to 212 μm in maximum diameter (mean = 134.1 μm, standard deviation = 25.9 μm, n = 60) and are oval to circular in shape are identified as *V. gracile* (e.g., Figs. 12A–O, 13A–F). Compaction has commonly resulted in a more ovate shape but the vesicle was likely originally spherical (Figs. 12A, K). Processes range from 8 to 36 μm in length. The longest and shortest process were measured on each specimen, as far as possible. The mean maximum process length is 20.9 μm (standard deviation = 6.2 μm, range 12–36 μm, n = 49), and the mean minimum process length is 15.9 μm (standard deviation = 5.1 μm, range = 8–28 μm, n = 49). The maximum process length as a proportion of vesicle maximum diameter ranges from 10 to 29% (mean = 16%, standard deviation = 5%, n = 49: Fig. 14A). The ranges of both maximum vesicle diameter and process length slightly exceed those considered diagnostic of this taxon by Xiao *et al.* (2014b), although the ratio of process length to vesicle diameter falls within the range they document. The processes in the Khesen examples range from 1 to 8 μm in thickness and are generally thickest where they connect with the vesicle, tapering distally and along branches (Figs. 12D, F). The thickness of processes tends to increase with their length ($R^2 = 0.46472$: Fig. 14C). Processes are hollow and continuous with the interior of the vesicle (Fig. 12D) although this may be obscured by redistribution of organic matter during degradation (Figs. 12F, H, K). Processes are separated by ~4–16 μm (mean = 7.9 μm, standard deviation = 2.7 μm, n = 49: Fig. 14B). Spacing is positively but weakly correlated to vesicle size ($R^2 = 0.20761$, Fig. 14D), and to process length ($R^2 = 0.32746$, Fig. 14E) and thickness ($R^2 = 0.51433$, Fig. 14F). Frequency distributions of both the maximum process length as a proportion of diameter and the maximum spacing between processes are multi-modal (Figs. 14A–B). The maximum process

length reveals modes at 8–10%, 14–16%, and 18–20%, and the maximum spacing at 4–6 μm and 10–12 μm. This suggests that *V. gracile* may represent more than one biological species.

The processes in *V. gracile* from Khesen show a complex pattern of branching (Figs. 12B, D, F, K–M, 13A–B) similar to that in *V. gracile* from the Doushantuo Formation, South China (Xiao *et al.*, 2014b). The first branch normally occurs about 50% along the length of the process. Bifurcation is the primary mode of branching and may lead to a feather-like appearance (Fig. 12B). Twisting of the processes on one specimen suggests flexibility (Figs. 13A–B). Some specimens (Figs. 12A–N, 13C–13F) show a light coloured region encompassing the processes which is presumably diagenetic in origin.

The preservation of *V. gracile* from Khesen varies considerably. Many specimens preserve minute details of the processes (Figs. 12A–F), which are usually dark in colour, whereas in others they are largely degraded (Figs. 12G, N). In a number of specimens, the vesicle is infilled with silica (Figs. 12C, E, H–L, N, 13A, C) and interior structures may be present (Figs. 12A, C, E, G, I–J, L, N). These interior areas of darker material have commonly contracted, presumably as a result of degradation. Specimen YPM 536777 contains an irregular mass of diagenetic phosphate (Fig. 12O).

Some specimens (Figs. 13C–F) contain numerous cell-like structures suggesting that *V. gracile* may represent a multicellular organism. The presence of such structures adds *Variomargosphaeridium* to a growing list of Ediacaran acanthomorph genera (e.g., *Eotylopalla, Megasphaera, Mengeosphaera,* and *Tianzhushania*) that display possible multicellular features (Xiao *et al.* 2014b).

Variomargosphaeridium aculeiparvum sp. nov.

(Figs. 15A–I)

Holotype. YPM 536786 (Figs. 15C–D).

Diagnosis. A species of *Variomargosphaeridium* with small to medium-sized vesicles (~100–170 μm maximum diameter) bearing numerous branching (successively dichotomously or ?multichotomously) processes that are <10 % of the vesicle maximum diameter in length.

Derivation of name. Latin *aculeus parvus*, meaning small spine or sting.

Material. Three specimens in thin-section YPM 536732, M618 33.0 A and two specimens in thin-section YPM 536736, M618 33.0 E.

Occurrence. Ediacaran, Khesen Formation, Khuvsgul Group, northern Mongolia.

Description. The vesicles are circular in thin-section (Figs. 15A, C, E, G) with a maximum diameter of 109–168 μm (mean = 146.4 μm, standard deviation = 22.7 μm, n = 5). Processes are short (4–12 μm in length, 3–7% of vesicle maximum diameter), broad at the base (up to 4 μm) and taper distally (to 1–2 μm) (Fig. 14H). The processes are no more than ~6 μm apart. They commonly branch beyond 50% of their length, normally successively bifurcating but sometimes multi-furcating (Figs. 15B, 15D, 15F–G). The processes of some specimens appear to show three branches which may curve away from the axis (Figs. 15D, F). The processes are hollow (Fig. 15H), although this may be obscured by degradation and redistribution of organic matter (Figs. 15D, F). There is commonly an opaque area within the vesicle (Figs. 15C, E, G) that is presumably a result of shrinkage or disaggregation of internal organic matter. Specimens may show the result of diagenesis including infilling with silica (Fig. 15G) and phosphatization (Fig. 15A), sometimes following significant degradation (Fig. 15I).

Remarks. We assign this form to *Variomargosphaeridium* based on the similarity of the processes to those in other species (Xiao *et al.*, 2014b). The length of the processes is <10 % of the vesicle maximum diameter, much less than in other species; those of *V. gracile* (10–33%), *V. litoschum* (10–20%), and *V. floridum* (14–19%) are relatively longer

(Moczydłowska & Nagovitsin 2012; Xiao *et al.* 2014b). Hence, we erect a new species, *V. aculeiparvum*. The generic diagnosis (Zang & Walter 1992; Xiao *et al.* 2014b) does not include process length as a proportion of vesicle diameter, and is therefore not emended.

Incertae Sedis

Genus ***Siphonophycus*** Schopf, 1968, emend. Knoll *et al.*, 1991

Type species. *Siphonophycus kestron* Schopf, 1968.

***Siphonophycus* spp.**

(Figs. 16A–G)

Material. *Siphonophycus* is present in a number of samples in addition to the four (YPM 536747, M618 32.0, YPM 536748, M618 33.0, YPM 536746, M602 176.0, and YPM 536749, M602 179.0) that have yielded the bulk of Khesen diversity.

Remarks. Tubular fossils that likely represent sheaths of cyanobacteria are assigned to *Siphonophycus*. *Siphonophycus* tubes are found occasionally in the Khesen phosphorites where they occur in three distinct arrangements: (1) concentrations of ~100s of criss-crossing individuals in a patchwork (e.g., Figs. 16A–B), (2) clusters of isolated individuals (e.g., Figs. 16C, E), and (3) clasts of layered microbial mat material (e.g., Figs. 16D, 16F–G). The clasts of microbial mat are on the order of several hundred micrometers in maximum dimension and usually elongate parallel to layers of *Siphonophycus* (Figs. 16D, F). The layers have commonly been rotated and folded (e.g., Fig. 16D), suggesting that the mat was ripped up and redeposited. These clasts may have been transported from an adjacent environment, as suggested by the rotated and folded nature, and by the rounded of some clasts (e.g, Fig. 16D).

Siphonophycus species are diagnosed on the basis of their maximum cross-sectional diameter in powers of two: 1–2, 2–4, 4–8, 9–16 μm etc. (Knoll *et al.* 1991), although studies

of large populations suggest that such distinctions may not be statistically robust (Anderson *et al.* 2017b). Degradation in the Khesen phosphorites (Fig. 16D) makes it difficult to determine maximum dimensions, or even to differentiate individual fossils in some mat clasts (Fig. 16F). Consequently, we do not assign *Siphonophycus* filaments to particular species, but note the likely presence of more than one.

Siphonophycus is also present in early diagenetic cherts of the Shuurgat and Zuun-Arts formations on the nearby Zavkhan Terrane in southwest Mongolia (Ragozina *et al.* 2007; Ragozina *et al.* 2010; Ragozina *et al.* 2016; Anderson *et al.* 2017b). *Siphonophycus*, particularly as well-developed microbial mats, is much more common in the Shuurgat cherts than in the Khesen phosphorites—it is the most abundant genus in Shuurgat rocks with thousands of reported specimens. This higher abundance may reflect different conditions for preservation or the influence of ecology and environmental setting on microbial communities.

Discussion

Comparison with other Doushantuo-Pertatataka-type microfossil assemblages

Doushantuo-Pertatataka-type acanthomorphic acritarchs are distributed worldwide and display a high level of diversity based largely on the varied morphology of their processes (Huntley *et al.* 2006). Consequently, they have been a focus for palaeontologists and biostratigraphers interested in subdividing the 94-million-year Ediacaran Period (Xiao *et al.* 2016). A survey orchestrated by the Subcommission on Neoproterozoic Stratigraphy showed biostratigraphy to be one of the most important ways to subdivide the Ediacaran (see fig. 2 in Xiao *et al.* 2016). However, the use of these fossils for biozonation and correlation has met with mixed success.

Successions in Australia have been subdivided into four acanthomorph Assemblage Zones: (1) *Appendisphaera barbata-Alicesphaeridium medsoidum-Gyalosphaeridium pulchrum*; (2) *Tanarium conoidium-Schizofusa risoria-Variomargosphaeridium litoschum*; (3) *Tanarium irregular-Ceratosphaeridium glaberosum-Multifronsphaeridium pelorium*; and (4) *Ceratosphaeridium mirabile-Distosphaera australica-Apodastoides verobturatus*, with an additional non-acanthomorph Assemblage Zone, *Leiosphaeridia jakutica-Leiosphaeridia crassa* (Grey 2005; Willman *et al.* 2006; Willman 2007; Willman & Moczydłowska 2008, 2011). Although successions on the East European Platform, and in India, Siberia, South China, and Svalbard share many fossil taxa with Australia, the Australian assemblage zones have not been identified elsewhere (Xiao *et al.* 2016). However, some progress has been made in reconciling the different records into an overarching biostratigraphic framework. An Assemblage Zone characterized by the fossil *Hocosphaeridium anozos* in the Doushantuo Formation, South China may correlate broadly with the four Australian acanthomorph zones. The *Hocosphaeridium anozos* Zone overlies a zone characterized by the fossil *Tianzhushania spinosa* (Liu *et al.* 2014; Xiao *et al.* 2014b), which occurs above the *c.* 635 Ma basal Ediacaran cap carbonate (McFadden *et al.* 2009). The nature of the succession between the *Tianzhushania spinosa* and *Hocosphaeridium anozos* zones is the subject of ongoing research and new data suggest that the two zones may overlap (Xiao *et al.* 2014b; Muscente *et al.* 2015; Xiao *et al.* 2016; Hawkins *et al.* 2017). Resolving these questions relies mainly on determining the relationship between the exposures of the Doushantuo Formation in Weng'an and the Yangtze Gorges (e.g., Xiao *et al.*, 2014b; Liu *et al.* 2014; Muscente *et al.* 2015).

Despite the difficulty of correlating occurrences of acanthomorphs on different continents, Doushantuo-Pertatataka-type acanthomorph assemblage zones have generally been regarded as pre-dating or synchronous with carbon isotope excursions equivalent to the Shuram carbon isotope excursion, which may be concurrent with the ~580 Ma Gaskiers

glaciation (Zhou *et al.* 2007; Xiao *et al.* 2016; Zhou *et al.*,2017). Acritarchs show a marked change in diversity and decrease in size after this time (e.g., Huntley *et al.* 2006). Doushantuo-Pertatataka-type acanthomorphs in the Doushantuo Formation itself in the Yangtze Gorges region occur below the EN3 negative $\delta^{13}C$ excursion, which is thought to correlate with the Shuram excursion (Zhou *et al.* 2017) and precedes an ash bed dated with U-Pb CA-TIMS on zircon at 551.09±1.02 Ma (Condon *et al.* 2005; Schmitz 2012). Xiao *et al.* (2014a) used available stratigraphic data and Lu-Hf and Pb-Pb dates on phosphorites (Barford *et al.* 2002; Chen *et al.* 2004; Chen *et al.* 2009c) to argue for a 600–582 Ma age for the Doushantuo assemblage.

The assumption that Doushantuo-Pertatataka-type acritarchs only occur prior to the Shuram interval has been challenged recently by several new discoveries. Golubkova *et al.* (2015) reported the occurrence of *Appendisphaera tenuis*, *Tanarium conoidium*, *T. pluripotensum*, and an unnamed species of *Tanarium* from putative latest Ediacaran strata on the East European Platform which, if their age is confirmed, would represent a significant extension of the stratigraphic record of both these genera. However, robust independent age constraints for these occurrences are lacking. Even in the Doushantuo Formation the assumption that Doushantuo-Pertatataka-type acritarchs pre-date the Shuram is being questioned. Ouyang *et al.* (2017) reported *Knollisphaeridium maximum*, *Mengeosphaera chadiensis*, possible examples of *M. cupsidata*, and several unidentified acanthomorphs from a new upper slope locality which postdates a negative $\delta^{13}C$ excursion thought to be equivalent to the EN3 elsewhere in the Doushantuo Formation, and thus the Shuram excursion.

The diversity of taxa in the upper Khesen Formation is comparable to that reported from most other Ediacaran successions globally, but it is substantially less than the more than 60 species known from the Doushantuo Formation (Cohen & Macdonald 2015). The

Mongolian assemblage shares several Doushantuo-Pertatataka-type acanthomorph taxa with the Doushantuo Formation: *Appendisphaera grandis*, *A. tenuis*, *Cavaspina basiconica*, and *Variomargosphaerdidum gracile* (Xiao *et al.* 2014b). The occurrence of *Variomargosphaeridium gracile* in the Khesen phosphorites is the only reported occurrence outside South China (Xiao *et al.* 2014b) but specimens assigned to *Dicrospinosphaera virgata* and *Dicrospinosphaera* sp. from Siberia (Vorob'eva *et al.* 2008; Sergeev *et al.* 2011) may also represent this taxon (Xiao *et al.* 2014b). *A. grandis* and *A. tenuis* occur not only in South China but in Australia and Siberia. *Appendisphaera fragilis,* which we report from the Khesen phosphorites, is absent in the Doushantuo Formation but is known from Siberia (Moczydłowska *et al.* 1993; Grey 2005; Moczydłowska 2005; Yin *et al.* 2007; Vorob'eva *et al.* 2008; Willman & Moczydłowska 2008; Chen *et al.* 2010; Golubkova *et al.* 2010; Sergeev *et al.* 2011; Xiao *et al.* 2014b). The Khesen phosphorites also share the multicellular taxon *Megasphaera* with the Doushantuo Formation (Xiao *et al.* 2014b). *Megasphaera* has recently been reported from the Ediacaran Chambaghat Formation in India (Shome *et al.* 2014) and similar fossils have been recovered from phosphatic intraclasts in the basal Denying Formation in China (Zhang & Zhang 2017). Whether or not these Denying intraclasts are reworked fragments of the underlying Doushantuo Formation remains to be tested. The specimens of *Megasphaera* from the Khesen Formation are generally smaller than those from elsewhere and mostly represent a new species, *Megasphaera minuscula*. Fossils reported from Member III of the Doushantuo Formation at Wangfenggang, Xiaofenghe, and Niuping by Liu *et al.* (2014) as "leiospheres with cellular inclusions" probably also represent *M. minuscula*. The Khesen *Megasphaera* specimens also include one which may represent *M. puncticulosa*—a taxon previously only described from the Doushantuo Formation.

The discovery that *Appendisphaera grandis*, *A. tenuis*, *Cavaspina basiconica*, and *Variomargosphaeridium gracile*, together with *Megasphaera* (the Khesen occurrence is only

the second reported outside South China), are present in the Khesen Formation as well as in the Doushantuo Formation (Anderson *et al.* 2017a) prompts regional palaeogeographic and stratigraphic comparisons with the Weng'an biota and that of Member III of the Doushantuo Formation in the Yangtze Gorges area. However, biostratigraphic comparison is restricted by the absence of *Tianzhushania spinosa* and *Hocosphaeridium anozos* in the Khesen Formation, the two species that are characteristic of the South China assemblage zones (Xiao *et al.* 2014b; Muscente *et al.* 2015; Xiao *et al.* 2016). Neither does the Mongolian assemblage include taxa characteristic of any of the four Australian zones (Grey 2005; Willman *et al.* 2006; Willman 2007; Willman & Moczydłowska 2008, 2011).

In the absence of biostratigraphic ties, lithostratigraphic and chemostratigraphic correlations provide independent age constraints on the fossiliferous horizons of the upper Khesen Formation. The lowermost phosphorite unit of the upper Khesen Formation can be correlated with the Zuun-Arts Formation of southwestern Mongolia, which includes the Proterozoic–Phanerozoic boundary (Macdonald & Jones 2011; Smith *et al.* 2016), and with the Zabit Formation of Siberia, which yields the latest Ediacaran fossil *Cloudina* (Grant 1990; Kherzaskova & Samygin 1992; Xiao *et al.* 2016). A sequence of granular phosphorites overlain by limestone and further bedded phosphorites characterizes both the upper Khesen Formation and the Zuun-Arts Formation (and the overlying basal Bayangol Formation) (Macdonald & Jones 2011; Smith *et al.* 2016). The carbon isotope excursion between the phosphorite rich successions in the upper Khesen Formation (Ilyin 2004; Vishnevskaya & Letnikova 2013, and fig. 2 herein), can therefore be correlated with the excursion that represents the Proterozoic–Phanerozoic boundary (Smith *et al.* 2016) in the Zuun-Arts. These geological and chemostratigraphic data indicate that the fossiliferous lowermost phosphorites of the upper Khesen Formation were deposited immediately prior to the Proterozoic–Phanerozoic boundary. This inference is supported by the position of both the Khesen and

Zuun-Arts phosphorites in foreland basins along the same margin. The geodynamics of foreland basin development (Sinclair & Naylor 2012) can result in diachronous deposition over a few million years through the migration of loads but not tens of millions of years: thus, the phosphorites on the different terranes are likely to be of similar age. Given the evidence that the age of the Khesen phosphorites lies close to the Proterozoic–Phanerozoic boundary, tens of millions of years younger than other Doushantuo-Pertatataka-type fossil assemblages, it is not surprising that biostratigraphic correlation is challenging.

A latest Ediacaran age for the Khesen fossils provides support for the extension of the stratigraphic range of *Appendisphaera tenuis* into the last few million years of the Ediacaran Period (e.g., Golubkova *et al.* 2015), and for the extension of *Cavaspina basiconica* beyond the Shuram carbon isotope excursion (Ouyang *et al.* 2017). The ranges of *A. grandis* and *A. fragilis*, and *Variomargosphaeridium gracile* are similarly extended as is that of the genus *Megasphaera*. The extension of Doushantuo-Pertatataka-type acritarchs into the last portion of the Ediacaran Period does not invalidate efforts to construct a robust biostratigraphy for pre-Shuram strata; none of the index fossils already used to define biozones are present in the Khesen assemblage.

Given that the Khesen assemblage is latest Ediacaran in age, we might expect similarities between it and the assemblage from the East European Platform described by Golubkova *et al.* (2015). The absence of *Cavaspina*, *Megasphaera* and *Variomargosphaeridium* from the East European Platform could be accounted for by different styles of fossilization. The East European Platform fossils are preserved as 2-dimensional carbonaceous compressions in shales whereas the upper Khesen fossils are phosphatized. Xiao *et al.* (2016) noted the difficulty of comparing acanthomorph assemblages preserved in different taphonomic modes: they require different preparation techniques (e.g., thin-section examination versus acid maceration), taxonomically useful

characters such as processes may degrade differently, and they may be confined to particular facies due to their ecology.

Conclusions

The upper Khesen discoveries add to a growing Neoproterozoic fossil record from Mongolian successions. The successions on the Zavkhan and Khuvsgul terranes chart the development of biological complexity during this crucial period, and are being combined with ever more comprehensive palaeoenvironmental data and robust geochronological constraints (Johnston *et al.* 2012; Rooney *et al.* 2015; Bold *et al.* 2016a; Bold *et al.* 2016b; Smith *et al.* 2016).

Early diagenetic cherts, which show petrographic similarities to those in early Ediacaran successions from India, South China, and Svalbard, and share taxa with two of these successions (India and South China) (Knoll 1992; Tiwari & Knoll 1994; Zhang *et al.* 1998; Xiao *et al.* 2010), were reported from the Shuurgat Formation on the Zavkhan Terrane (Anderson *et al.* 2017b). The Shuurgat Formation lies below the major Ediacaran unconformity and yields strontium isotopic compositions consistent with early Ediacaran strata elsewhere (Macdonald *et al.* 2009; Macdonald 2011; Macdonald & Jones 2011; Bold *et al.* 2016b). The younger Zuun-Arts Formation, also on the Zavkhan Terrane and correlative with the Khesen Formation, preserves macroscopic algal carbonaceous compressions in shale (Dornbos *et al.* 2016), possible acanthomorphic acritarchs and microscopic multicellular fossils in silicified and phosphatic sediments (Ragozina *et al.* 2007; Ragozina *et al.* 2010; Ragozina *et al.* 2016), and simple bed-planar trace fossils (Goldring & Jensen 1996; Smith *et al.* 2016). The Zuun-Arts Formation has also yielded putative sponge spicules (Brasier *et al.* 1997) although their nature and even biogenicity has been questioned (Zhou *et al.* 1998).

Fossils from the early Cambrian of Mongolia are better known. The Bayangol and Salaagol formations preserve diverse small shelly fossils: anabaritids, protoconodonts, cap-shaped fossils, *Salanacus*, hyolithelminthes, coeloscleritophorans, tommotiids, orthothecimorphs, molluscs, and calcareous brachiopods (Voronin *et al.* 1982; Endonzhamts & Lkhasuren 1988; Dorjnamjaa *et al.* 1993; Brasier *et al.* 1996; Esakova & Zhegallo 1996; Goldring & Jensen 1996; Khomentovsky & Gibsher 1996; Kruse *et al.* 1996; Maloof *et al.* 2010; Smith *et al.* 2016;). Archaeocyathids are confined to the Salaagol Formation (Smith *et al.* 2016; Pruss *et al.* 2017). The Bayangol and Salaagol formations also host a variety of trace fossils (Goldring & Jensen 1996).

The fossil assemblage of the lowermost phosphorites of the upper Khesen Formation adds to the growing evidence (e.g., Bosak *et al.* 2011a; Bosak *et al.* 2011b; Cohen *et al.* 2015; Dornbos *et al.* 2016; Bold *et al.* 2016b; Smith *et al.* 2016; Anderson *et al.* 2017b; Moore *et al.* 2017) that Mongolian sequences are of critical importance to unravelling the transition from a Proterozoic world of microbes to a Phanerozoic world where complex organisms are geobiological agents.

Acknowledgments

We thank U. Bold who organized the logistics in northern Mongolia. This research benefited from discussions with A. Knoll and L. Tarhan. S. Butts and J. Utrup managed the collections of the Yale Peabody Museum of Natural History Division of Invertebrate Paleontology. The work was supported by a Geological Society of America ExxonMobil Student Geoscience Grant, the National Aeronautics and Space Administration (NASA) Astrobiology Institute [NNA13AA90A] *Foundations of Complex Life, Evolution, Preservation and Detection on Earth and Beyond*, the Yale Institute for Biospheric Studies,

and the Yale Peabody Museum of Natural History. RPA was supported by NASA Headquarters under the Earth and Space Science Fellowship Program [NNX14AP10H]. We are grateful to H. Agić and S. Xiao, whose helpful reviews improved this article.

References

Adl, S. M., Simpson, A. G. B., Lane, C. E., Lukeš, J. Bass, D., Bowser, S. S., Brown, M. W., Burki, F., Dunthorn, M., Hampl, V., Heiss, A., Hoppenrath, M., Lara, E., Gall, L. L., Lynn, D. H., McmAnus, H., Mitchell, E. A. D., Mozley-Stanridge, S. E., Parfrey, L. W., Pawlowski, J., Rueckert, S., Shadwick, L., Schoch, C. L., Smirnov, A. & Spiegel, F. W. 2012. The revised classification of eukaryotes. *The Journal of Eukaryotic Microbiology*, **59**(5), 429–514.

Anderson, R. P., Macdonald, F. A., Jones, D. S., McMahon, S. & Briggs, D. E. G. 2017a. Dosuhantuo-type microfossils from latest Ediacaran phosphorites of northern Mongolia. *Geology*, **45**(12), 1079–1082.

Anderson, R. P., McMahon, S., Bold, U., Macdonald, F. A. & Briggs, D. E. G. 2017b. Palaeobiology of the early Ediacaran Shuurgat Formation, Zavkhan Terrane, southwestern Mongolia. *Journal of Systematic Palaeontology*, **11**, 947–968

Asseyeva, E. A. 1974. On spiral and ring-like structures from the Upper Precambrian of Podolia. *Paleontology Sbornik*, **2**, 95–98. [In Russian].

Bailey, J. V., Joye, S. B., Kalanetra, K. M., Flood, B. E. & Corsetti, F. A. 2007. Evidence of giant sulphur bacteria in Neoproterozoic phosphorites. *Nature*, **445**, 198–201.

Barford, G. H., Alberède, F. Knoll, A. H., Xiao, S., Télouk, P., Frei, R. & Baker, J. 2002. New Lu-Hf and Pb-Pb age constraints on the earliest animal fossils. *Earth and Planetary Science Letters*, **201**, 203–212.

Bengtson, S., Cunningham, J. A., Yin, C. & Donoghue, P. C. J. 2012. A merciful death for the "earliest bilaterian", Vernanimalcula. *Evolution and Development*, **14**, 412–427.

Bold, U., Crowley, J. L., Smith, E. F., Sambuu, O. & Macdonald, F. A. 2016a. Neoproterozoic to early Paleozoic tectonic evolution of the Zavkhan terrane of Mongolia: Implications for continental growth in the Central Asian orogenic belt. *Lithosphere*, **9**(6), 729–750.

Bold, U., Macdonald, F. A., Smith, E. F., Crowley, J. L., Minjin, C. & Dorjnamjaa, D. 2013. Elevating the Neoproterozoic Tsaagan-Olom Formation to a Group. *Mongolian Geoscientist*, **39**(5), 90–94.

Bold, U., Smith, E. F., Rooney, A. D., Bowring, S. A., Buchwaldt, R., Dudás, F. Ö., Ramexani,, J., Corwley, J. L., Schrag, D. P. & Macdonald, F. A. 2016b. Neoproterozoic stratigraphy of the Zavkhan Terrane of Mongolia: The backbone for Cryogenian and early Ediacaran chemostratigraphic records. *American Journal of Science*, **316**(1), 1–63.

Bosak, T., Lahr, D. J. G., Pruss, S. B., Macdonald, F. A., Dalton, L. & Matys, E. D. 2011a. Agglutinated tests in post-Sturtian cap carbonates of Namibia and Mongolia. *Earth and Planetary Science Letters*, **308**(1–2), 29–40.

Bosak, T., Macdonald, F. A., Lahr, D. J. G. & Matys, E. D. 2011b. Putative Cryogenian ciliates from Mongolia. *Geology*, **39**(12), 1123–1126.

Brasier, M. D., Green, O. & Shields-Zhou, G. 1997. Ediacaran sponge spicule clusters from southwestern Mongolia and the origins of the Cambrian fauna. *Geology*, **25**(4), 303–306.

Brasier, M. D., Shields-Zhou, G., Kuleshov, V. N. & Zhegallo, E. A. 1996. Integrated chemo- and biostratigraphic calibration of early animal evolution: Neoproterozoic–early Cambrian of southwest Mongolia. *Geological Magazine*, **133**(4), 445–485.

Burzin, M. B. 1995. Late Vendian helicoids filamentous microfossils. *Paleontological Journal*, **29**, 1–34.

Butterfield, N. J. 2011. Terminal developments in Ediacaran embryology. *Science*, **334**, 1655–1656.

Butterfield, N. J., Knoll, A. H. & Swett, K. 1994. Paleobiology of the Neoproterozoic Svanbergfjellet Formation, Spitsbergen. *Fossils and Strata* **34**, 1–84.

Chen, D. F., Dong, W. Q., Zhu, B. Q. & Chen, X. P. 2004. Pb-Pb ages of Neoproterozoic Doushantuo phosphorites in South China: Constraints on early metazoan evolution and glaciation events. *Precambrian Research*, **132**(1–2), 123–132.

Chen, J.-Y. 2004. *The Dawn of the Animal World*. Jiangsu Science and Technology Press, Nanjing, China, 366 pp.

Chen, J.-Y., Bottjer, D. J., Davidson, E. H., Li, G., Gao, F., Cameron, A. R., Hadfield, M. G., Xian, D.-C., Tafforeau, P., Jia, Q.-J., Sugiyama, H. & Tang, R. 2009a. Phase contrast synchrotron X-ray microtomography of Ediacaran (Doushantuo) metazoan microfossils: Phylogenetic diversity and evolutionary implications. *Precambrian Research*, **173**, 191–200.

Chen, J.-Y., Bottjer, D. J., Li, G., Hadfield, M. G., Gao, F., Cameron, A. R., Zhang, C.-Y., Xian, D.-C., Tafforeau, P., Liao, X. & Yin, Z.-J. 2009b. Complex embryos displaying bilaterian characters from Precambrian Doushantuo phosphate deposits Weng'an, Guizhou, China. *Proceedings of the National Academy of Sciences*, **106**, 19056–19060.

Chen, L., Xiao, S., Pang, K., Zhou, C. & Yuan, X. 2014. Cell differentiation and germ-soma separation in Ediacaran animal embryo-like fossils. *Nature*, **516**, 238–241.

Chen, M. & Liu, K. 1986. The geological significance of newly discovered microfossils from the upper Sinian (Doushantuo age) phosphorites. *Scientia Geologica Sinica*, **1**, 46–53.

Chen, S., Yin, C., Liu, P., Gao, L., Tang, F. & Wang, Z. 2010. Microfossil assemblage from chert nodules of the Ediacaran Doushantuo Formation in Zhangcunping, Northern Yichang, South China. *Acta Geologica Sinica*, **84**, 70–77.

Chen, Y.-Q., Jiang, S.-Y., Ling, H.-F. & Yang, J.-H. 2009c. Pb-Pb dating of black shales from the Lower Cambrian and Neoproterozoic strata, South China. *Chemie der Erde*, **69**(2), 183–189.

Cohen, P. A., Knoll, A. H. & Kodner, R. B. 2009. Large spinose microfossils in Ediacaran rocks as resting stages of early animals. *Proceedings of the National Academy of Sciences*, **106**, 6519–6524.

Cohen, P. A. & Macdonald, F. A. 2015. The Proterozoic record of eukaryotes. *Paleobiology*, **41**(4), 610–632.

Cohen, P. A., Macdonald, F. A., Pruss, S. B., Matys, E. & Bosak, T. 2015. Fossils of putative marine algae from the Cryogenian glacial interlude of Mongolia. *Palaios*, **30**, 238–247.

Condon, D., Zhu, M., Bowring, S. A., Wang, A., Yang, A. & Jin, Y. 2005. U-Pb ages from the Neoproterozoic Doushantuo Formation, China. *Science*, **308**, 95–98.

Cook, P. J. & Shergold, J. H. *Phosphate deposits of the of the world, Volume 1: Proterozoic and Cambrian phosphorites*. Cambridge University Press, Cambridge, 391 pp.

Cunningham, J. A., Vargas, K., Yin, Z., Bengtson, S. & Donoghue, P. C. J. 2017. The Weng'an Biota (Doushantuo Formation): An Ediacaran window on soft-bodied and mutlicellular microorganisms. *Journal of the Geological Society*, **174**, 793–802.

Dong, L., Xiao, S., Shen, B., Zhou, C., Li, G. & Yao, J. 2009. Basal Cambrian microfossils from the Yangtze Gorges Area (South China) and the Aksy Area (Tarim Block, Northwestern China). *Journal of Paleontol*ogy, **83**(1), 30–44.

Donov, N. A., Edemsky, H. B. & Ilyin, A. V. 1967. Cambrian phosphorites of Mongolia Popular Republic. *Sovetskaya Geologia*, **3**, 55–60. [In Russian].

Dorjnamjaa, D., Bat-Ireedui, Y. A., Dashdavaa, Z. & Soelmaa, D. 1993. *Precambrian-Cambrian Geology of the Dzavkhan Zone*. Department of Earth Sciences, University of Oxford, Oxford, 36 pp.

Dornbos, S. Q., Bottjer, D. J., Chen, J.-Y., Gao, F., Oliveri, P. & Li, C. W. 2006. Environmental controls on the taphonomy of phosphatized animals and animal embryos from the Neoproterozoic Doushantuo Formation, southwest China. *Palaios*, **21**, 3–14.

Dornbos, S. Q., Oji, T., Kanayama, A. & Gonchigdorj, S. 2016. A new Burgess Shale-type deposit from the Ediacaran of western Mongolia. *Scientific Reports*, **6**, 23438.

Downie, C. & Sarjeant, W. A. S. 1963. On the interpretation and status of some hystrichosphere genera. *Palaeontolog*y, **6**, 83–96.

Eisenack, A. 1958. *Tasmanites* Newton 1875 und *Leiosphaeridia* n.g. als Gattungen de Hystrichosphaeridea. *Palaeontographica A*, **110**, 1–19. [In German].

Endonzhamts, Z. & Lkhasuren, B. 1988. Stratigrafi ya pgranichnykh tolsch dokembriya i kembriya Dzabkhanskoy zony. Pp 150–162 in V.V. Khomentovsky and V. Y.Shenfil' (eds) *Pozdniy dokembriy i ranniy paleozoy Sibiri, Rifey i vend.. Institut Geologii i Geofi ziki, Sibirskoe Otdelenie*. Akademiya Nauk, SSSR, Novosibirsk. [In Russian].

Esakova, N. V. & Zhegallo, E. A. 1996. Statigrafaya i fauna nizhnego Kembriya Mongolii (Lower Cambrian stratigraphy and fauna of Mongolia). *Sovmestnaya Sovetsko-Mongol'skaya Paleontologicheskaya Ekspeditsiya*, **46**, 208 pp. [In Russian].

Goldring, R. & Jensen, S. 1996. Trace fossils and biofabrics at the Precambrian-Cambrian boundary interval in western Mongolia. *Geological Magazine*, **133**(4), 403–415.

Golovenok, V. K. & Belova, M. Y. 1989. Microfossils of Obruchevella parva Reitlinger from Vendian deposits of Lena River basin. *Doklady AN USSR*, **306**, 190–193. [In Russian].

Golubic, S. & Barghoorn, E. S. 1977. Interpretation of microbial fossils with special reference to the Precambrian. Pp. 1–14 in E. Flügel (ed) *Fossil Algae: Recent results and development*. Springer-Verlag, Berlin, Germany.

Golubkova, E. Y., Raevskaya, E. G. & Kuznetsov, A. B. 2010. Lower Vendian microfossil assemblages of East Siberia: Significance for solving regional stratigraphic problems. *Stratigraphy and Geological Correlation*, **18**, 353–375.

Golubkova, E. Y., Zaitseva, T. S., Kuznetsov, A. B., Dovzhikova, E. G. & Maslov, A. V. 2015. Microfossils and Rb-Sr age of glauconite in the key section of the Upper Proterozoic of the northeastern part of the Russian Plate (Keltmen-1 Borehole). *Doklady Earth Sciences*, **462**(2), 547–551.

Grant, S. W. F. 1990. Shell structure and sitribution of *Cloudina*, a potential index fossil for the terminal Proterzoic. *American Journal of Science*, **290**, 261–294.

Grey, K. 2005. Ediacaran palynology of Australia. *Memoirs of the Australasian Association of Palaeontologists*, **31**, 1–439.

Hagadorn, J. W., Xiao, S. H., Donoghue, P. C. J., Bengtson, S., Gostling, N. J., Pawlowska, M., Raff, E. C., Raff, R. A., Turner, F. R., Chongyu, Y., Zhou, C., Yuan, X., McFeely, M. B., Stampanoni, M. & Nealson, K. H. 2006. Cellular and subcellular structure of Neoproterozoic embryos. *Science*, **314**, 291–294.

Hawkins, A. D., Xiao, S., Jiang, G., Wang, X. & Shi, X. 2017. New biostratigraphic and chemostratigraphic data from the Ediacaran Doushantuo Formation in intra-shelf and

upper slope facies of the Yangtze platform: Implications for biozonation of acanthomoprhic acritarchs in South China. *Precambrian Research*, **300**, 28–39.

Huldtgren, T., Cunningham, J. A., Yin, C., Stampanoni, M., Marone, F., Donoghue, P. C. J. & Bengtson, S. 2011. Fossilized nuclei and germination structures identify Ediacaran "animal embryos" as encysting protists. *Science*, **334**(6063), 1696–1699.

Huntley, J. W., Xiao, S. & Kowaleski, M. 2006. 1.3 billion years of acritarch history: An empircal morphospace approach. *Precambrian Research*. **144**, 52–68.

Ilyin, A. V. 1973. *Khubsugul phsphorite-bearing basin*. Geolgicheskiy Institut, Doklady Akademiya Nauk SSSR, Moscow, Russia, 167 pp. [In Russian].

Ilyin, A. V. 2004. The Khubsugul phosphate-bearing basin: New data and concepts. *Lithology and Mineral Resources*, **39**, 454–467.

Ilyin, A. V., Zaitsev, N. S. & Bjamba, Z. 1986. Proterozoic and Cambrian phosphorites—deposits: Khubsugul, Mongolian People's Republic. Pp. 162–174 in P. J. Cook and J. H. Shergold (eds) *Phosphate Deposits of the World, Volume 1: Proterozoic and Cambrian Phosphorites*. Cambridge University Press, Cambridge.

Ilyin, A. V. & Zhuraveleva, I. T. 1968. On the boundary between the Cambrian and the Precambrian at Prikhusugulie (Mongolian PR). *Doklady Akademiya Nauk SSS*R, **182**, 1164–1166. [In Russian].

Jankauskas, T. V., Mikhailova, N. S. & Hermann, T. N. 1989. *Mikrofossilii Dokembriya SSSR*. Nauka, Leningrad, Russia, 190 pp. [In Russian].

Johnston, D. T., Macdonald, F. A., Gill, B. C., Hoffman, P. F. & Schrag, D. P. 2012. Uncovering the Neoproterozoic carbon cycle. *Nature*, **483**(7389), 320–U110.

Joshi, H. & Tiwari, M. 2016. *Tianzhushania spinosa* and other large acanthomorphic acritarchs of the Ediacaran Period from the Infrakrol Formation, Lesser Himalaya, India. *Precambrian Research*, **286**, 325–336.

Kherzaskova, T. N. & Samygin, S. G. 1992. Tectonic conditions in the East Sayan Vendian-Middle Cambrian terrigenous carbonate association. *Geotectonics*, **26**, 445–458.

Khomentovsky, V. V. & Gibsher, A. S. 1996. The Neoproterozoic–Lower Cambrian in northern Govi-Altay, western Mongolia: Regional setting, lithostratigraphy and biostratigraphy. *Geological Magazine*, **133**(4), 371–390.

Knoll, A. H. 1992. Vendian microfossils in metasedimentary cherts of the Scotia Group, Prins Karls Forland, Svalbard. *Palaeontology*, **35**(4), 751–774.

Knoll, A. H., Swett, K. & Mark, J. 1991. Paleobiology of a Neoproterozoic tidal flat/lagoonal complex: The Draken conglomerate formation, Spitsbergen. *Journal of Paleontology*, **65**(4), 531–570.

Kolosov, P. N. 1984. *Upper Precambrian microorganisms from the east of Siberian Platform, Yakutsk*. Yakutskii Filial Sibirskogo Otdeleniya AN SSSR, Russia 84 pp. [In Russian].

Kolosova, S. P. 1991. Late Precambrian acanthomorphic acritarchs from the eastern Siberian Platform. *Algologiya*, **1**, 53–59. [In Russian].

Korobov, M. N. 1980. Lower Cambrian biostratography and miomeroid trilobites of the Lower Cambrian of Mongolia. Pp. 5–108 in V.V. Menner and S.V. Meyen (eds) *Lower Cambrian and Carboniferous biostratigraphy of Mongolia, Volume 26*. Trudy Sovmestnou Sovetsoko-Mongol-skoy Paleontologicheskoy Exspeditsii, Moscow. [In Russian].

Kruse, P. D., Gandin, A., Debrenne, F. & Wood, R. 1996. Early Cambrian bioconstructions in the Zavkhan Basin of western Mongolia. *Geological Magazine*, **133**(4), 429–444.

Kuzmichev, A. B. & Larionov, A. N. 2011. The Sarkhoi Group in East Sayan: Neoproterozoic (~770-800 Ma) volcanic belt of the Andean type. *Russian Geology and Geophysics*, **52**(7), 685–700.

Liu, P., Xiao, S. H., Yin, C., Chen, S., Zhou, C. &Li, M. 2014. Ediacaran acanthomorphic acritarchs and other microfossils from chert nodules of the Upper Doushantuo Formation in the Yangtze Gorges Area, South China. *Journal of Paleontology*, **88**, 1–139.

Luo, Q., Wang, F. & Wang, Y. 1982. Uppermost Sinian lowest Cambriab age microfossils from Qingzhen-Zhikin County, Guizhou Province. *Bulletin Tianjin Institute of Geology and Mineral Resources, Chinese Academy of Sciences*, **6**, 23–41.

Macdonald, F. A. 2011. The Tsagaan Oloom Formation, southwestern Mongolia. Pp. 331–337 in E. Arnaud, G. P. Halverson, and G. Shields-Zhou (eds) *The Geological Record of Neoproterozoic Glaciations*. Geological Society of London, London.

Macdonald, F. A. & Jones, D. S., 2011. The Khubsugul Group, northern Mongolia. Pp 339–345 in E. Arnaud, G. P. Halverson, and G. Shields-Zhou (eds) *The Geological Record of Neoproterozoic Glaciations*. Geological Society of London, London.

Macdonald, F. A., Jones, D. S. & Schrag, D. P. 2009. Stratigraphic and tectonic implications of a newly discovered glacial diamictite-cap carbonate couplet in southwestern Mongolia. *Geology*, **37**(2), 123–126.

Maloof, A. C., Porter, S. M., Moore, J. L., Dudás, F. Ö, Bowring, S. A., Higgins, J. A., Fike, D. A. & Eddy, M. P. 2010. The earliest Cambrian record of animals and ocean geochemical change. *Geological Society of America Bulletin*, **122**(11–12), 1731–1774.

Martin, D., Briggs, D. E. G. & Parkes, R. J. 2003. Experimental mineralization of invertebrate eggs and the preservation of Neorpoterozoic embryos. *Geology*, **31**(1), 30–42.

Martin, D., Briggs, D. E. G. & Parkes, R. J. 2004. Experimental attachment of sediment particles to invertebrate eggs and the preservation of soft-bodied fossils. *Journal of the Geological Society of London*, **161**, 735–738.

McFadden, K. A., Xiao, S. H., Zhou, C. & Kowaleski, M. 2009. Quantitative evaluation of the biostratigraphic distribution of acanthomorphic acritarchs in the Ediacaran Doushantuo Formation in the Yangtze Gorges area, South China. *Precambrian Research*, **173**, 170–190.

Moczydłowska, M. 2005. Taxonomic review of some Ediacaran acritarchs from the Siberian Platform. *Precambrian Research*, **136**, 170–190.

Moczydłowska, M. & Nagovitsin, K. E. 2012. Ediacaran radiation of organic-walled microbiota recorded in the Ura Formation, Patom Uplift, East Siberia. *Precambrian Research*, **198–199**, 1–24.

Moczydłowska, M., Vidal, G. & Rudavskaya, V. A. 1993. Neoproterozoic (Vendian) phytoplankton from the Siberia platform, Yakutia. *Palaeontology*, **36**, 495–521.

Moore, K. R., Bosak, T., Macdonald, F. A., Lahr, D. J. G., Newman, S., Settens, C. & Pruss, S. B. 2017. Biologically agglutinated eukaryotic microfossil from Cryogenian cap carbonates. *Geobiology*, **15**(4), 499–515.

Muscente, A. D., Hawkins, A. D. & Xiao, S. H. 2015. Fossil preservation through phosphatization and silicification in the Ediacaran Doushantuo Formation (South China): A comparative synthesis. *Palaeogeography Palaeoclimatology Palaeoecology*, **434**, 46–62.

Muscente, A. D., Schiffbauer, J. D., Broce, J., Laflamme, M., O'Donnell, K., Boag, T. H., Meye, M., Hawkins, A. D., Huntley, J. W., McNamara, M. E., MacKenzie, L. A., Stanley, G. D., Hinman, N. W., Hofmann, M. H. & Xiao, S. 2017. Exceptionally preserved fossil assemblages through geologic time and space. *Gondwana Research*, **48**, 164–188.

Nagovitsin, K. E. 2000. Silicified microbiotas of the Upper Riphean of the Yenisei Ridge: News in paleontology and stratigraphy. *Geology and Geophysic*, **41**, 7–31.

Nagovitsin, K. E., Faizullin, M. S. & Yakshin, M. S. 2004. New forms of Baikalian acanthomorphytes from the Ura Formation if the Patom Uplift, East Siberia. *Geologiya e Geofishka*, **45**, 7–19. [In Russian].

Naumova, S. N. 1949. Spory nizhnego kembriya. *Izvestiya Akademii Nauk SSSR, Seriya Geologicheskaya*, **4**, 49–56. [In Russian].

Oehler, D. Z. 1977. Microflora of the H. Y. C. Pyrite Shale Member of the Barney Creek Formation (McArthur Group), middle Proterozoic of northern Australia. *Alcheringa*, **1**, 315–349.

Oehler, D. Z. 1978. Microflora of the middle Proterozoic Balbrini Dolomite (McArthur Group) of Australia. *Alcheringa*, **2**, 269–309.

Osokin, P. V. & Tyzhinov, A. V. 1998. Precambrian tilloids of the Oka-Khubsugul phosphorite-bearing basin (Eastern Sayan, Northwestern Mongolia). *Lithology and Mineral Resources*, **33**, 142–154.

Porter, S. M. 2011. The rise of predators. *Geology*, **39**(6), 607–608.

Porter, S. M. 2016. Tiny vampires in ancient seas: Evidence for predation via perforation in fossils from the 780–740 million-year-old Chuar Group, Grand Canyon, USA. *Proceedings of the Royal Society B: Biological Scienc*es, **283**(1831), 20160221

Porter, S. M. & Riedman, L. A. 2016. Systematics of organic-walled microfossils from the ca. 780-740 Ma Chuar Group, Grand Canyon, Arizona. *Journal of Paleontology*, **90**(5), 815–853.

Pruss, S. B., Dwyer, C. H., Smith, E. F., Macdonald, F. A. & Tosca, N. J. 2017. Phosphatzied early Cambrian archaeocyaths and small shelly fossils (SSFs) of southwestern Mongolia. *Palaeogeography, Palaeoclimatology, Palaeoecology*.

Raff, E. C., Vilinski, F. R., Turner, P. C., Donoghue, P. C. J. & Raff, R. A. 2006. Experimental taphonomy shows the feasibility of fossil embryos. *Proceedings of the National Academy of Sciences*, **103**, 5846–5851.

Ragozina, A. L., Dorjnamjaa, D., Krayushkin, A. V. & Serezhnikova, E. A. 2007. Body fossils and trace fossils from the Vendian-Cambrian section of Dzabkhan Zone Western Mongolia. Pp. 57–64 in M. A. Semikhatov (ed) *The Rise and Fall of the Vendian (Ediacaran) Biota Origin of a Modern Biosphere*. Proceedings of the International Symposium (IGCP Project 493), Moscow, GEOS, Russia.

Ragozina, A. L., Dorjnamjaa, D., Krayushkin, A. V., Serezhnikova, E. A. & Enkhbaator, B. 2010. Vendian-Cambrian biota of the Western Mongolia. Pp. 187–190 in V.M. Podobina (ed) *Evolution of Life on the Earth*. Proceedings of the IV International Symposium, TML-Press, Tomsk, Russia.

Ragozina, A. L., Dorjnamjaa, D., Serezhnikova, E. A., Zaitseva, L. V. & Enkhbaator, B. 2016. Association of macro- and microfossils in the Vendian (Ediacaran) postglacial successions in Western Mongolia. *Stratigraphy and Geological Correlation*, **24**(3), 242–251.

Reitlinger, E. A. 1948. Cambrian foraminifera of Yakutsk. *Byulleten Moskovskogo Obshchestva Ispytateleja Priody, Otdel Geologicheskii*, **23**, 77–81. [In Russian].

Reitlinger, E. A. 1959. *Atlas of microscopic organic remains and problematica of ancient deposits of Siberia*. Academiya Nauk SSSR, Moscow, Russia, 62 pp. [In Russian].

Rooney, A. D., Strauss, J. V., Brandon, A. D. & Macdonald, F. A. 2015. A Cryogenian chronology: Two long-lasting synchronous Neoproterozoic glaciations. *Geology*, **43**(5), 459–462.

Schmitz, M. D. 2012. Appendix 2 - Radiometric ages used in the GTC2012. Pp. 1045–1082 in F. Gradstein, J. Ogg, M. D. Schmitz, and G. Ogg (eds) *The Geological Time Scale 2012*. Elsevier, Boston, USA.

Schopf, J. W. 1968. Microflora of the Bitter Springs Formation, Late Precambrian, central Australia. *Journal of Paleontology*, **42**, 651–688.

Schopf, J. W., Sergeev, V. N. & Kudryavtsev, A. B. 2015. A new approach to ancient microorganisms: taxonomy, paleoecology, and biostratigraphy of the Lower cambrian Berkuta and Chulaktau microbiotas of South Kazakhstan. *Journal of Paleontology*, **89**(5), 695–729.

Sergeev, V. N., Knoll, A. H. & Vorob'eva, N. G. 2011. Ediacaran microfossils from the Ura Formation, Baikal-Patom uplift, Siberia: Taxonomy and biostratigraphic significance. *Journal of Paleontology*, **85**, 987–1011.

Sergeev, V. N., Sharma, M. & Shukla, Y. 2012. Proterozoic fossil cyanobacteria. *The Palaeobotanist*, **61**, 189–358.

Sharma, M., & Shukla, Y. 2012. Occurrence of helically coiled microfossils Obruchevella in the Owk Shale of the Kurnool Group and its significance. *Journal of Earth System Science*, **121**(3), 755–768.

Shome, S., Mathur, V. K., Nath, S., Xiao, S. & Broce, J. 2014. Occurrence of Neoproterozoic animal embryos in the Chmabghat Formation of Himachal Lesser Himalaya, India. *Current Science*, **106**(6), 813–815.

Shukla, R. & Tiwari, M. 2014. Ediacaran acanthomorphic acritarchs from the Outer Krol Belt, Lesser Himalaya, India: Their significance for global correlation. *Palaeoworld*, **23**, 209–224.

Sinclair, H. & Naylor, M. 2012. Foreland basin subsidence driven by topographic growth versus plate subduction. *Geological Society of America Bulletin*, **124**, 368–379.

Smith, E. F., Macdonald, F. A., Petach, T. A., Bold, U. & Schrag, D. P. 2016. Integrated stratigraphic, geochemical, and paleontological late Ediacaran to early Cambrian records from southwestern Mongolia. *Geological Society of America Bulletin*, **128**, 442–468.

Song, X. 1984. *Obruchevella* from the Early Cambrian Meishucunian Stage of the Meishucun section, Jinning, Yunnan, China. *Geological Magazine*, **121**, 179–183.

Spjeldnaes, N. 1963. A new fossil (*Papillomembrana* sp.) from the Upper Precambrian of Norway. *Nature*, **200**, 63–64.

Spjeldnaes, N. 1967. Fossils from pebbles of the Biskopåsen Formation in southern Norway. *Norges Geologiske Undersok*else, **251**, 53–82.

Tiwari, M. & Knoll, A. H. 1994. Large acanthomorphic acritarchs from the Infrakrol Formation of the Lesser Himalaya and their stratigraphic significance. *Journal of Himalayan Geology*, **5**(2), 193–201.

Turner, R. E. 1984. Acritarchs from the type area of the Ordovician Caradoc Series, Shropshire, England. *Palaeontographica Abeitlung B*, **190**, 87–157.

Vidal, G. 1990. Giant acanthomorphic acritarchs from the upper Proterozoic in southern Norway. *Palaeontology*, **33**, 287–298.

Vishnevskaya, I. A. & Letnikova, E. F. 2013. Chemostratigraphy of the Vendian-Cambrian carbonate sedimentary cover of the Tuva-Mongolian microcontinent. *Russian Geology and Geophysics*, **54**(6), 567–586.

Vorob'eva, N. G., Sergeev, V. N. & Chumakov, N. M. 2008. New finds of early Vendian microfossils in the Ura Formation: Revision of the Patom Supergorup age, middle Siberia. *Doklady Earth Sciences*, **419A**, 411–416.

Vorob'eva, N. G., Sergeev, V. N. & Knoll, A. H. 2009a. Neoproterozoic microfossils from the margin of the east European platform and the search for a biostratigraphic model of lower Ediacaran rocks. *Precambrian Research*, **173**, 163–169.

Vorob'eva, N. G. 2009b. Neoproterozoic microfossils from the northeastern margin of the East European Platform. *Journal of Paleontology*, **83**, 161–169.

Voronin, Y. L., Voronova, L. G., Grigor'eva, N. V., Drozdova, N. A., Zhegallo, E. A., Zhuralev, A. Y., Ragozina, A. L., Rosanov, A. Y., Sayutina, T. A., Syosev, V. A. & Fonin, V. D. 1982. *The Precambrian/Cambrian boundary in the geosynclinal areas (the reference section of Salaany-Gol, MPR)*. Trudy Sovmestnoy Sovetsoko-Mongol'skoy Paleontologicheskoy Exspeditsii, Akademia Nauk SSSR, Moscow, 180 pp. [In Russian].

Wang, F., Zhang, X. & Guo, R. 1983. The Sinian microfossils from Jinning, Yunnan, southwest China. *Precambrian Research*, **23**, 133–175.

Willman, S. 2007. Acritarchs and their potential in Ediacaran biostratigraphy - Examples from the Officer Basin, Australia. *Communicações Geológicas*, **94**, 81–92.

Willman, S. & Moczydłowska, M. 2008. Ediacaran acritarch biota from the Giles 1 drillhole, Officer Basin, Australia, and its potential for biostratigraphic correlation. *Precambrian Research*, **162**, 498–530.

Willman, S. & Moczydłowska, M. 2011. Acritarchs in the Ediacaran of Australia - Local or global significance? Evidence from the Lake Maurice West 1 drillcore. *Review of Palaeobotany and Palynology*, **166**, 12–28.

Willman, S., Moczydłowska, M. & Grey, K. 2006. Neoproterozoic (Ediacaran) diversification of acritarchs: A new record from the Murnaroo 1 drillcore, eastern Officer Basin, Australia. *Review of Palaeobotany and Palynology*, **139**, 17–39.

Xiao, S. & Knoll, A. H. 1999. Fossil preservation in the Neoproterozoic Doushantuo phosphorite Lagerstätte, South China. *Lethaia*, **32**, 219–240.

Xiao, S. & Knoll, A. H. 2000. Phosphatized animal embryos from the Neoproterozoic Doushantuo Formation at Weng'An, Guizhou, South China. *Journal of Paleontology*, **74**(5), 767–788.

Xiao, S., Knoll, A. H., Schiffbauer, J. D., Zhou, C. & Yuan, X. 2012. Comment on "Fossilized Nuclei and Germination Structures Identify Ediacaran 'Animal Embryos' as Encysting Protists". *Science*, **335**(6073), 1169.

Xiao, S., Knoll, A. H., Yuan, X. & Pueschel, C. M. 2004. Phosphatized multicellular algae in the Neoproterozoic Doushantuo formation, China, and the early evolution of florideophyte red algae. *American Journal of Botany*, **91**(2), 214–227.

Xiao, S., Muscente, A. D., Chen, L., Zhou, C.-M., Schiffbauer, J. D., Wood, A. D., Polys, N. F. & Yuan, X.-L. 2014a. The Weng'an biota and the Ediacaran radiation of multicellular eukaryotes. *National Science Review*, **1**, 498–520.

Xiao, S., Narbonne, G. M., Zhou, C.-M., Laflamme, M., Grazhdankin, D. V., Moczydłowska-Vidal, M. & Cui, H. 2016. Towards an Ediacaran Time Scale. Problems, Protocols, and Prospects. *Episodes*, **39**(4), 540–555.

Xiao, S., Schiffbauer, J. D., McFadden, K. A. & Hunter, J. 2010. Petrographic and SIMS pyrite sulfur isotope analyses of Ediacaran chert nodules: Implications fro microbial processes in pyrite rim formation, silicifcation, and exceptional fossil preservation. *Earth and Planetary Science Letters*, **297**, 481–495.

Xiao, S., Zhang, Y. & Knoll, A. H. 1998. Three-dimensional preservation of algae and animal embryos in a Neoproterozoic phosphorite. *Nature*, **391**, 553–558.

Xiao, S., Zhou, C., Liu, P., Wang, D. & Yuan, X. 2014b. Phosphatized acanthomorphic acritarchs and related microfossils from the Ediacaran Doushantuo Formation at Weng'an (south China) and their implications for biostratigraphic correlation. *Journal of Paleontology*, **88**, 1–67.

Xiao, S., Zhou, K. & Yuan, X. 2007. Undressing and redressing Ediacaran embryos. *Nature*, **446**, E9–10.

Xue, Y., Tang, T., Yu, C. & Zhou, C. 1995. Large spheroidal chlorophyta fossils from the Doushantuo Formation phosphoric sequene (late Sinian), central Guizhou, South China. *Acta Palaeontologica Sinica*, **34**(6), 688–706.

Yakschin, M. S. & Luchinina, V. A. 1981. New data on fosssilized algae of the Oscillatoriaceae (Kirchn.) Elenkin family. Pp. 28–34 in *The Precambrian-Cambrian boundary deposits of the Siberian platform*. Nauka, Novosibirsk, Russia. [In Russian].

Yankauskas, T. V. 1989. *Precambrian microfossils of the USSR*. Nauka, Leningrad, Russia, 188 pp. [In Russian].

Yin, C., Bengtson, S. & Yue, Z. 2004. Silicified and phosphatized Tianzhushanian, spheroidal microfossils of possible animal origin from the Neoproterozoic of South China. *Acta Palaeontologica Polonica*, **49**, 1–12.

Yin, C. & Liu, G. 1988. Micropaleofloras of the Sinian system of Hubei. Pp. 91–100, 170–180 in *The Sinian System of Hubei*, China University of Geosciences Press, Wuhan, China. [In Chinese[.

Yin, L., Zhu, M., Knoll, A. H., Yuan, X., Zhang, J. & Hu, J. 2007. Doushantuo embryos preserved inside diapause egg cysts. *Nature*, **446**, 661–663.

Yin, Z., Liu, P., Li, G., Tafforeau, P. & Zhu, M. 2014. Biological and taphonomic implications of Ediacaran fossil embryos undergoing cytokinesis. *Gondwana Research*, **25**, 1010–1026.

Yin, Z., Zhu, M., Davidson, E. H., Bottjer, D. J., Zhao, F. & Tafforeau, P. 2015. Sponge grade body fossil with cellular resolution dating 60 Myr before the Cambrian. *Proceedings of the National Academy of Sciences*, **112**(12), E1453–1460.

Yin, Z.-J., Zhu, M., Tafforeau, P., Chen, J.-Y., Liu, P. & Li, G. 2013. Early embryogenesis of potential bilaterian animals with polar lobe formation from the Ediacaran Weng'an Biota, South China. *Precambrian Research*, **225**, 44–57.

Yoon, H. S., Müller, K. M., Sheath, R. G., Ott, F. D. & Battacharya, D. 2006. Defining the major lineages of red algae (Rhodophyta). *Journal of Phycology*, **42**(2), 482–292.

Yuan, X. & Hofmann, H. J. 1998. New microfossils from the Neoproterozoic (Sinian) Doushantuo Formation, Weng'an, Guizhou Province, southwestern China. *Alcheringa*, **22**, 189–122.

Yuan, X., Xiao, S., Yin, L., Knoll, A. H., Zhou, C. & Mu, X. 2002. *Doushantuo Fossils: Life on the eve of animal radiation*. China University of Science and Technology, Hefei, China, 71 pp.

Zang, W. & Walter, M. R. 1992. Late Proterozoic and Cambrian microfossils and biostratigraphy, Amadeus Basin, central Australia. *Memoirs of the Australasian Association of Palaeontologists*, **12**, 1–132.

Zhang, Y., Yin, L., Xiao, S. & Knoll, A. H. 1998. Permineralized fossils from the terminal Proterozoic Doushantuo Formation, South China. *The Paleontological Society Memoir*, **50**, 1–52.

Zhang, Y. & Zhang, X. 2017. New Megashpaera-like microfossils reveal their reproductive strategies. *Precambrian Research*, **300**, 141–150.

Zhou, C., Brasier, M. D. & Xue, Y. 2001. Three-dimensional phosphatic preservation of giant acritarchs from the terminal Proterozoic Doushnatuo Formation in Guizhou and Hubei provinces, South China. *Palaeontology*, **44**, 1157–1178.

Zhou, C., Xiao, S., Wang, W., Guan, C., Ouyang, Q. & Chen, Z. 2017. The stratigraphic complexity of the middle Ediacaran carbon isotope record in the Yangtze Gorges area, South China, and its implications for the age and chemostratigraphic significance of the Shuram excursion. *Precambrian Research*, **288**, 23–38.

Zhou, C., Xie, G., McFadden, K. A., Xiao, S. & Yuan, X. 2007. The diversification and extinction of Doushantuo-Pertatataka acritarchs in South China: Causes and biostratigraphic significance. *Geological Journal*, **42**, 229–262.

Zhou, C., Yuan, X. & Xiao, S. 2002. Phosphatized biotas from the Neoproterozoic Doushantuo Formation on the Yangtze Platform. *Chinese Science Bulletin*, **47**, 1918–1924.

Zhou, C.-M., Yuan, X.-L. & Xue, Y-S. 1998. Sponge spicule-like pseudofossils from the Neoproterozoic Toushantuo formation in Weng'an, Guizhou, China. *Acta Micropalaeontologica Sinica*, **15**, 380–384.

Figure Captions

Figure 1. Geological setting of the Khesen fossil assemblage. **A,** Generalized map showing the geographic location of the Zavkhan and Khuvsgul terranes within Mongolia. **B,** Geological map of the western margin of Lake Khuvsgul highlighting the fossiliferous phosphorite and showing the location of major measured sections.

Figure 2. Stratigraphic setting of the Khesen fossil assemblage, showing relationships between the Zavkhan and Khuvsgul terranes. **A,** Generalized Cryogenian–Cambrian stratigraphy on the Zavkhan Terrane, (MU = Maikhan Uul Formation, BG = Bayangol Formation). **B,** Generalized stratigraphy on the Khuvsgul terrane. **C,** Stratigraphy and carbon isotopes at Ongoluk Gol. **D,** Stratigraphy and carbon isotopes at Khesen Gol. **E,** Stratigraphy and carbon isotopes at Urandush Uul. Tie points are marked. In particular, the Proterozoic–Phanerozoic boundary is shown as a dashed line. Major fossil horizons are indicated.

Figure 3. Flat-bed scan of thin-section showing granular Khesen phosphorites, YPM 536729, M618 32.0 B. Scale bar is 3 mm.

Figure 4. *Obruchevella*, **A–B** and **D–G** photomicrographs from thin-section, **C** is scanning electron micrograph of acid-extracted specimen. In this and subsequent figure legends YPM numbers are given, in addition to rock sample/thin section identifications and, where appropriate, England Finder coordinates for all illustrated sedimentary structures, microfossils and populations. **A,** *O. delicata*, YPM 536750, M602 176.0 B, E47/0. **B,** *O. magna*, YPM 536778, M618 33.0 A, F42/3. **C,** *O. magna*, YPM 538075, from YPM 536747, M618 32.0. **D,** *O. magna* in cross-section, YPM 536779, M618 33.0 A, F42/3. **E,** *O. parvissima*, YPM 536792, M618 33.0 C, S59/3. **F,** *O. parvissima*, YPM 536793, M618 33.0 C, M60/0. **G,** *O.valdaica*, YPM 536780, M618 33.0 A, F42/3. Scale bars are 50 μm in all images.

Figure 5. *Archaeophycus yunnanensis*. **A–E,** photomicrographs from thin-section, YPM 536754, M618 32.0 D, P55/0. **F,** scanning electron micrograph of YPM 538070, from YPM 536747, M618 32.0. Scale bars are 30 μm in all images.

Figure 6. Photomicrographs of *Appendisphaera* from thin-section. **A–D,** *A. grandis*, YPM 536755, M618 32.0 D, K41/3. **D** shows processes extended beyond the darker region which is bounded by a rim (also evident in **B**). The darker area in **C** shows a more transitional gradation. **E,** *A. fragilis*, YPM 536781, M618 33.0 A, O70/0. **F,** *A. fragilis* showing processes that converge to give the impression of larger tapering processes, YPM 536751, M602 179.0 A, M44/0. **G,** *A. fragilis*, YPM 536782, M618 33.0 A, V69/0. **H–I,** *A. tenuis*, YPM 536756, M618 32.0 C, Q62/1. Scale bars are 50 μm in A, E, and H; 30 μm in B, D, G, and I; and 10 μm in C, and F.

Figure 7. Scanning electron micrographs of *Cavaspina basiconica*, all fossils extracted from YPM 536747, M618 32.0. **A,** YPM 538072. **B,** YPM 538071, showing a hole in vesicle wall (arrow). **C,** YPM 538722. **D,** YPM 538723, with possible internal structures. **E,** YPM 538724, with a ruptured vesicle. **F,** YPM 538725 with folds on the vesicle surface. Scale bars are 100 μm in all images.

Figure 8. Photomicrographs of *Leiosphaeridia* in thin-section. **A–E,** *L. crassa*, YPM 536757, M618 32.0 D, D44/2; various specimens show internal structures. **F,** *L. jacutica*, YPM 536758, M618 32.0 C, W72/2, infilled with silica. **G–H,** *L. jacutica*, YPM 536752, M602 179.0 B J65/0, showing subspherical structures, each <3 μm, within interior. **I,** *L. jacutica*, YPM 536812, M618 33.0 H, G58/4, infilled with silica. **J,** *L. jacutica*, YPM 536759, M618 32.0 C, W60/4, showing interior structures. **K,** *L. jacutica*, YPM 536790, M618 33.0 B, N68/4, infilled with silica. **L,** *L. tenuissima*, YPM 536763, M618 32.0 B F68/2, showing interior structures. **M,** *L. tenuissima*, YPM 536764, M618 32.0 B, R74/0, surrounded by diagenetic halo. **N,** Frequency distribution of maximum vesicle diameters. Scale bars are 50

μm in A, B, F, G, I–M; 30 μm in C–D, and H; and 20 μm in E.

Figure 9. Photomicrographs of well-preserved specimens of *Megasphaera minuscula* in thin-section. **A–B,** YPM 536783, M618 32.0 A, P54/0. **C–D,** YPM 536784, M618 33.0 A, P45/0. **E–F,** YPM 536794, M618 33.0 C, O61/3. **G–I,** YPM 536765, M618 32.0 B, C65/2. **J–K,** YPM 536766, M618 32.0 B, D51/0. **L–M,** YPM 536810, M618 33.0 G, Y43/1. **N,** Frequency distribution of maximum vesicle diameter for both well- and poorly-preserved specimens. Scale bars are 50 μm in A, C, E, G, and L; 30 μm in B, D, F, H–J, and M, and 20 μm in K.

Figure 10. A–H, J–K, Photomicrographs of poorly-preserved specimens of *Megasphaera minuscula* in thin-section. **A,** YPM 536785, M618 33.0 A, Z48/0. **B,** YPM 536791, M618 33.0 B, S70/2. **C,** YPM 536795, M618 33.0 C, U58/3. **D,** YPM 536813, M618 33.0 H, B48/0. **E,** YPM 536811, M618 33.0 G, D40/2, shrunken interior with granular structures covering interior. **F,** YPM 536804, M618 33.0 D, Z53/3, crescent-shaped area vacated by shrunken interior infilled by silica. **G,** YPM 536796, M618 33.0 C, L54/0, outer vesicle is missing, possible traces of it breaking away above the specimen. **H,** YPM 536805, M618 33.0 D, Z69/4, outer vesicle is missing. **I,** Photomicrograph of *L. tenuissima* in thin-section, YPM 536760, M618 32.0 B, Z63/0, analogue for one-cell stage. **J,** YPM 536761, M618 32.0 C, Q70/4, with phosphatized external vesicle. **K,** YPM 536762, M618 32.0 C, Z54/4, with possible sculptured exterior vesicle and diagenetic halo. **L,** internal cells mean maximum diameter external versus vesicle mean maximum diameter. Scale bars are 50 μm in all images.

Figure 11. Scanning electron micrographs of *Megasphaera minuscula* **(A–J)** *and M.* ?*punticulosa* **(K–L)**, acid-extracted from YPM 536747, M618 32.0. **A,** YPM 538726, may

alternatively represent a leiosphere. **B,** YPM 538727, may alternatively represent a leiosphere. **C,** YPM 538718, with thick wall. **D,** YPM 538074, with thick wall. **E–H,** YPM 538073, YPM 538728, YPM 538729, YPM 538719, all with diagenetic phosphate in the interior. **I,** YPM 538721, with raised equatorial band. **J,** YPM 538797, with single large "stalk" and crater (arrow). **K–L,** YPM 538720, with exterior ornamentation. Scale bars are 50 μm in A, B, D, L; 100 μm in C, E, G, I, J, K; and 200 μm in F, I.

Figure 12. Photomicrographs of *Variomargosphaeridium gracile* in thin-section. **A–N,** show a diagenetic halo between processes. **A–B,** YPM 536800, M618 32.0 A, Y61/0, some infilling with silica, internal structure, and feather-like processes. **C–D,** YPM 536801, M618 32.0 A, K41/2, infilled with silica and internal structure. **E–F,** YPM 536802, M618 32.0 A, Q69/1, infilled with silica and internal dark area. **G,** YPM 536803, M618 32.0 A, U51/4, with internal structure. **H,** YPM 536767, M618 32.0 B, L65/0, infilled with silica. **I,** YPM 536768, M618 32.0 B, Z40/4, with internal structure and silica replacement. **J,** YPM 536770, M618 32.0 C, P55/0, infilled with silica and some internal structure. **K,** YPM 536774, M618 32.0 D, M75/3, infilled with silica. **L–M,** YPM 536775, M618 32.0 D, O52/4, infilled with silica and some internal structure. **N,** YPM 536776, M618 32.0 A, B39/0 infilled with silica with some internal structure. **O,** YPM 536777, M618 32.0 A, U51/4, with diagenetic phosphate infill. Scale bars are 50 μm in A, C, E, G–L, N, and O, 30 μm in B and F; and 20 μm in M.

Figure 13. Photomicrographs of further *Variomargosphaeridium gracile* in thin-section. **A–B,** YPM 536771, M618 32.0 C, F67/1, with slender processes that are long with respect to the vesicle diameter and show evidence of twisting. **C–D,** YPM 536769, M618 32.0 B, L69/0, with internal cell-like structures (?multicellular). **E,** YPM 536772, M618 32.0 C, H71/3, with internal cell-like structures (?multicellular). **F,** YPM 536773 M618 32.0 C, K48/4, with

internal cell-like structures (?multicellular). Scale bars are 50 μm in A, C, E, and F; and 30 μm in B and D.

Figure 14. Dimensions of *Variomargosphaeridium gracile*. **A,** frequency histogram of maximum process length as a percentage of vesicle maximum diameter diameter. **B,** frequency histogram of process spacing. **C,** process maximum thickness versus process maximum length. **D,** process spacing versus vesicle maximum diameter. **E,** process spacing versus process maximum length. **F,** process spacing versus process maximum thickness.

Figure 15. Photomicrographs of *Variomargosphaeridium aculeiparvum* in thin-section. **A–B,** YPM 536806, M618 33.0 E, Y6/0, with diagenetic phosphate mineralization infilling vesicle interior. **C–D,** YPM 536786, M618 33.0 A, F58/3, with shrunken interior and silica infill. **E–F,** YPM 536787, M618 33.0 A, L50/1, with shrunken interior and silica infill. **G–H,** YPM 536807, M618 33.0 E, P42/3, with silica infill and interior structure. **I** YPM 536788, M618 33.0 A, E51/4, degraded example. Scale bars are 50 μm in A, C, E, G, and I; 30 μm in B and F; and 20 μm in D and H.

Figure 16. Photomicrographs of *Siphonophycus* in thin-section. **A–B,** YPM 536789, M618 33.0 A, X53/1, inter-woven criss-crossing mat texture with high concentration of *Siphonophycus* fossils. **C,** YPM 536797, M618 33.0 C, U53/2, filaments with thickened walls, likely a result of degradation. **D,** YPM 536808, M618 33.0 F, C54/0, large layered microbial mat clast rounded and folded around itself includes various *Siphonophycus* species. **E,** YPM 536798, M618 33.0 C, U53/2. **F,** YPM 536808, M618 33.0 F, C54/0, microbial mat texture from clast in D with *Siphonophycus* filaments. **G,** YPM 536799, M618 32.0 B, J63/2, small microbial fragment with *Siphonophycus* filaments. Scale bars are 100 μm in D; 50 μm

in A, C, and G; and 30 μm in B, E, and F.

Tables

Table 1. Biostratigraphic chart of the upper Khesen Formation showing taxa reported from the four most diverse samples and their relative abundance within the assemblage. R = rare (isolated individuals, only a few specimens). C = common (10s of individuals).

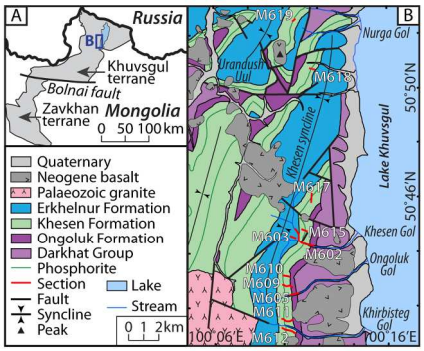

Figure 1. Geological setting of the Khesen fossil assemblage. A, Generalized map showing the geographic location of the Zavkhan and Khuvsgul terranes within Mongolia. B, Geological map of the western margin of Lake Khuvsgul highlighting the fossiliferous phosphorite and showing the location of major measured sections.

82x232mm (300 x 300 DPI)

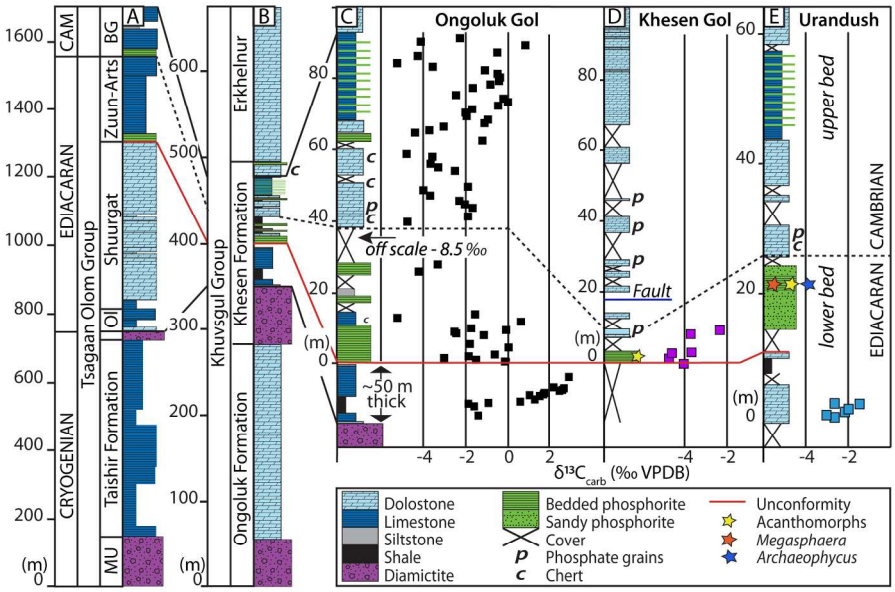

Figure 2. Stratigraphic setting of the Khesen fossil assemblage, showing relationships between the Zavkhan and Khuvsgul terranes. A, Generalized Cryogenian–Cambrian stratigraphy on the Zavkhan Terrane, (MU = Maikhan Uul Formation, BG = Bayangol Formation). B, Generalized stratigraphy on the Khuvsgul terrane. C, Stratigraphy and carbon isotopes at Ongoluk Gol. D, Stratigraphy and carbon isotopes at Khesen Gol. E, Stratigraphy and carbon isotopes at Urandush Uul. Tie points are marked. In particular, the Proterozoic–Phanerozoic boundary is shown as a dashed line. Major fossil horizons are indicated.

173x232mm (300 x 300 DPI)

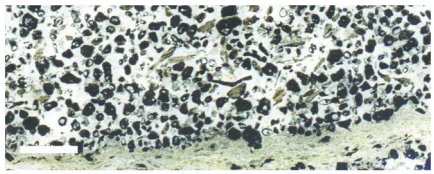

Figure 3. Flat-bed scan of thin-section showing granular Khesen phosphorites, YPM 536729, M618 32.0 B. Scale bar is 3 mm.

82x232mm (300 x 300 DPI)

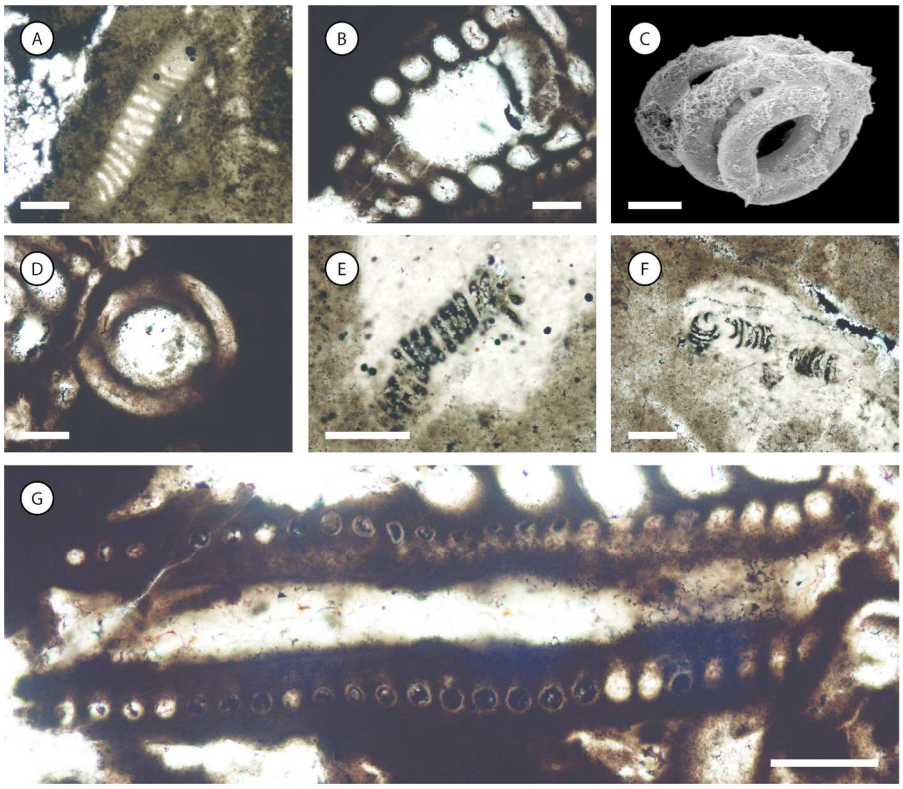

Figure 4. *Obruchevella*, A–B and D–G photomicrographs from thin-section, C is scanning electron micrograph of acid-extracted specimen. In this and subsequent figure legends YPM numbers are given, in addition to rock sample/thin section identifications and, where appropriate, England Finder coordinates for all illustrated sedimentary structures, microfossils and populations. A, *O. delicata*, YPM 536750, M602 176.0 B, E47/0. B, *O. magna*, YPM 536778, M618 33.0 A, F42/3. C, *O. magna*, YPM 538075, from YPM 536747, M618 32.0. D, *O. magna* in cross-section, YPM 536779, M618 33.0 A, F42/3. E, *O. parvissima*, YPM 536792, M618 33.0 C, S59/3. F, *O. parvissima*, YPM 536793, M618 33.0 C, M60/0. G, *O.valdaica*, YPM 536780, M618 33.0 A, F42/3. Scale bars are 50 μm in all images.

173x232mm (300 x 300 DPI)

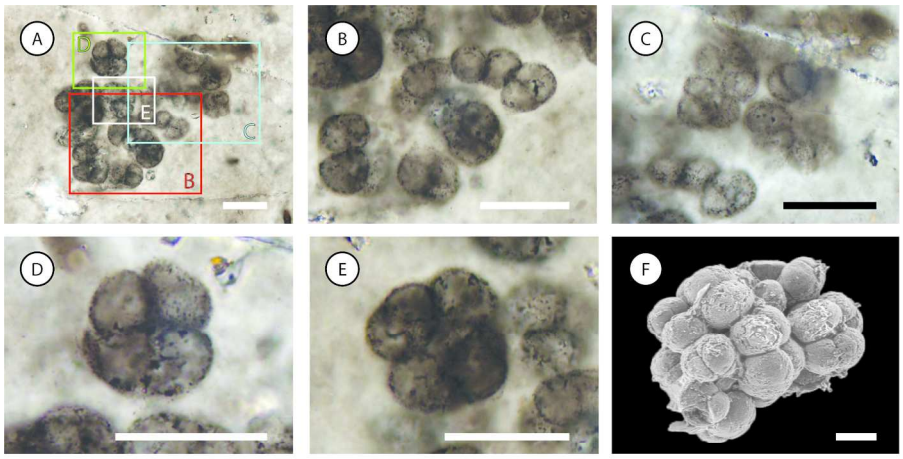

Figure 5. *Archaeophycus yunnanensis*. A–E, photomicrographs from thin-section, YPM 536754, M618 32.0 D, P55/0. F, scanning electron micrograph of YPM 538070, from YPM 536747, M618 32.0. Scale bars are 30 μm in all images.

173x232mm (300 x 300 DPI)

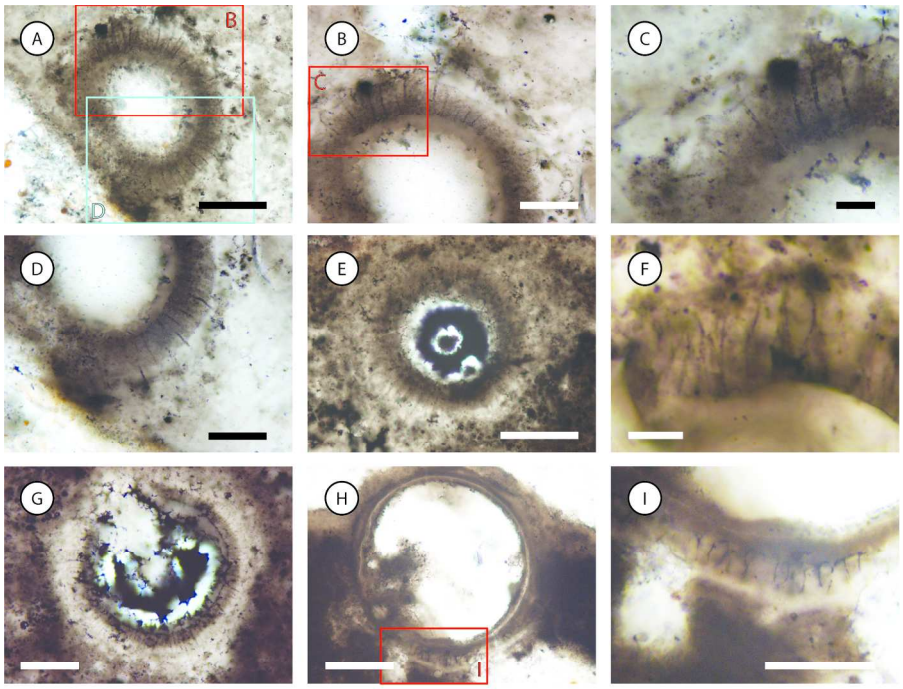

Figure 6. Photomicrographs of *Appendisphaera* from thin-section. A–D, *A. grandis*, YPM 536755, M618 32.0 D, K41/3. D shows processes extended beyond the darker region which is bounded by a rim (also evident in B). The darker area in C shows a more transitional gradation. E, *A. fragilis*, YPM 536781, M618 33.0 A, O70/0. F, *A. fragilis* showing processes that converge to give the impression of larger tapering processes, YPM 536751, M602 179.0 A, M44/0. G, *A. fragilis*, YPM 536782, M618 33.0 A, V69/0. H–I, *A. tenuis*, YPM 536756, M618 32.0 C, Q62/1. Scale bars are 50 μm in A, E, and H; 30 μm in B, D, G, and I; and 10 μm in C, and F.

173x232mm (300 x 300 DPI)

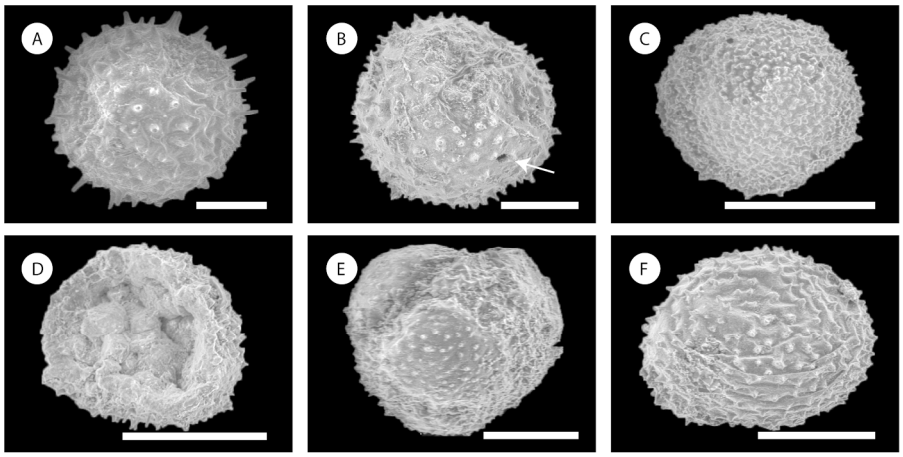

Figure 7. Scanning electron micrographs of *Cavaspina basiconica*, all fossils extracted from YPM 536747, M618 32.0. A, YPM 538072. B, YPM 538071, showing a hole in vesicle wall (arrow). C, YPM 538722. D, YPM 538723, with possible internal structures. E, YPM 538724, with a ruptured vesicle. F, YPM 538725 with folds on the vesicle surface. Scale bars are 100 μm in all images.

173x232mm (300 x 300 DPI)

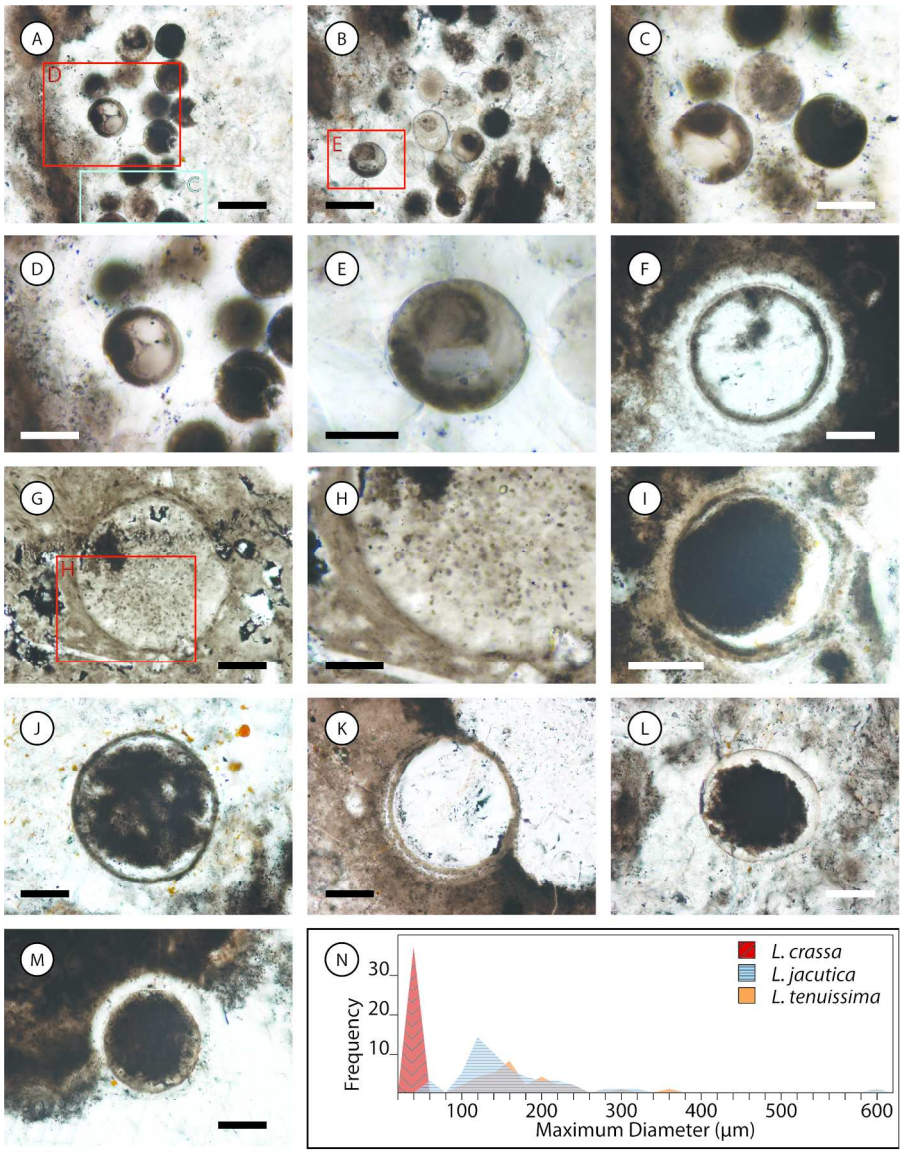

Figure 8. Photomicrographs of *Leiosphaeridia* in thin-section. A–E, *L. crassa*, YPM 536757, M618 32.0 D, D44/2; various specimens show internal structures. F, *L. jacutica*, YPM 536758, M618 32.0 C, W72/2, infilled with silica. G–H, *L. jacutica*, YPM 536752, M602 179.0 B J65/0, showing subspherical structures, each <3 µm, within interior. I, *L. jacutica*, YPM 536812, M618 33.0 H, G58/4, infilled with silica. J, *L. jacutica*, YPM 536759, M618 32.0 C, W60/4, showing interior structures. K, *L. jacutica*, YPM 536790, M618 33.0 B, N68/4, infilled with silica. L, *L. tenuissima*, YPM 536763, M618 32.0 B F68/2, showing interior structures. M, *L. tenuissima*, YPM 536764, M618 32.0 B, R74/0, surrounded by diagenetic halo. N, Frequency distribution of maximum vesicle diameters. Scale bars are 50 µm in A, B, F, G, I–M; 30 µm in C–D, and H; and 20 µm in E.

173x232mm (300 x 300 DPI)

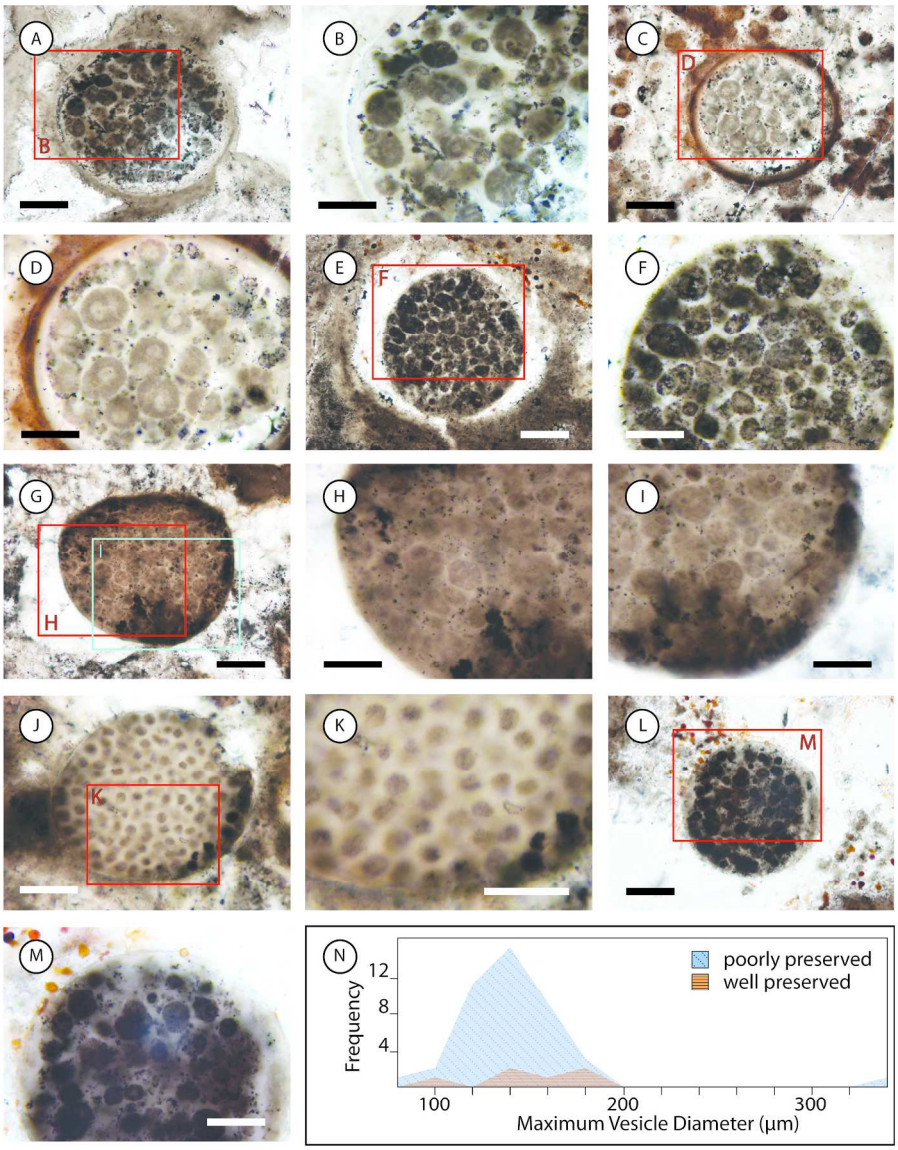

Figure 9. Photomicrographs of well-preserved specimens of *Megasphaera minuscula* in thin-section. A–B, YPM 536783, M618 32.0 A, P54/0. C–D, YPM 536784, M618 33.0 A, P45/0. E–F, YPM 536794, M618 33.0 C, O61/3. G–I, YPM 536765, M618 32.0 B, C65/2. J–K, YPM 536766, M618 32.0 B, D51/0. L–M, YPM 536810, M618 33.0 G, Y43/1. N, Frequency distribution of maximum vesicle diameter for both well- and poorly-preserved specimens. Scale bars are 50 µm in A, C, E, G, and L; 30 µm in B, D, F, H–J, and M, and 20 µm in K.

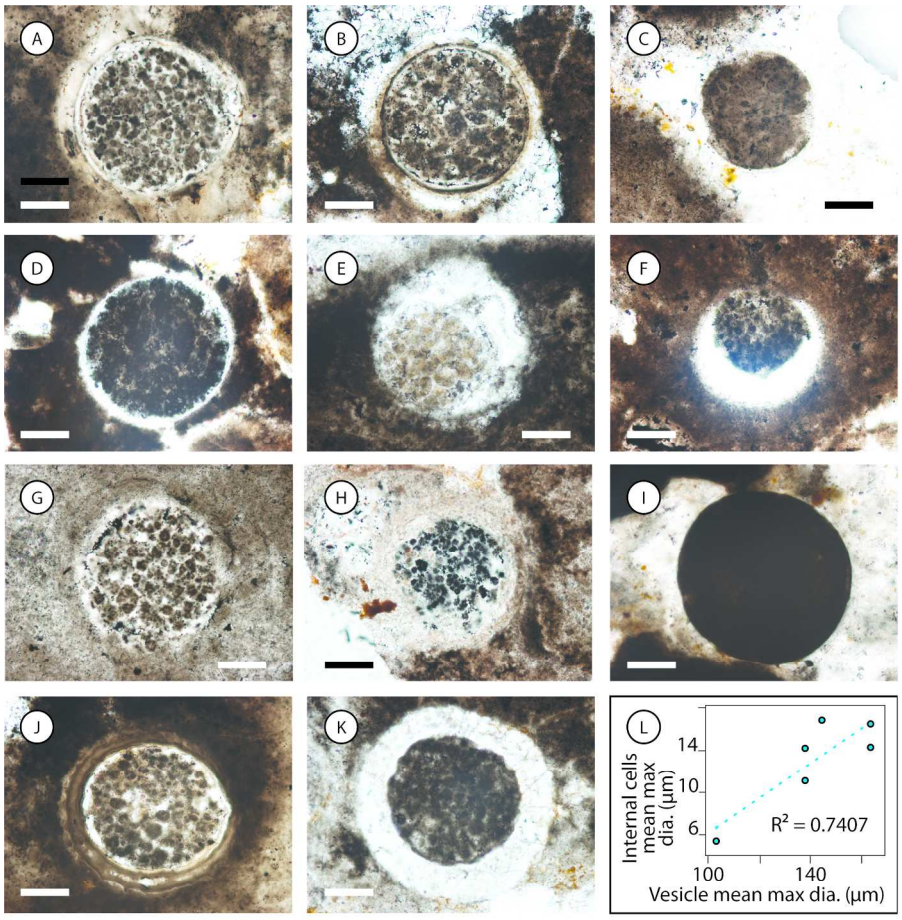

Figure 10. A–H, J–K, Photomicrographs of poorly-preserved specimens of *Megasphaera minuscula* in thin-section. A, YPM 536785, M618 33.0 A, Z48/0. B, YPM 536791, M618 33.0 B, S70/2. C, YPM 536795, M618 33.0 C, U58/3. D, YPM 536813, M618 33.0 H, B48/0. E, YPM 536811, M618 33.0 G, D40/2, shrunken interior with granular structures covering interior. F, YPM 536804, M618 33.0 D, Z53/3, crescent-shaped area vacated by shrunken interior infilled by silica. G, YPM 536796, M618 33.0 C, L54/0, outer vesicle is missing, possible traces of it breaking away above the specimen. H, YPM 536805, M618 33.0 D, Z69/4, outer vesicle is missing. I, Photomicrograph of *L. tenuissima* in thin-section, YPM 536760, M618 32.0 B, Z63/0, analogue for one-cell stage. J, YPM 536761, M618 32.0 C, Q70/4, with phosphatized external vesicle. K, YPM 536762, M618 32.0 C, Z54/4, with possible sculptured exterior vesicle and diagenetic halo. L, internal cells mean maximum diameter external versus vesicle mean maximum diameter. Scale bars are 50 µm in all images.

173x232mm (300 x 300 DPI)

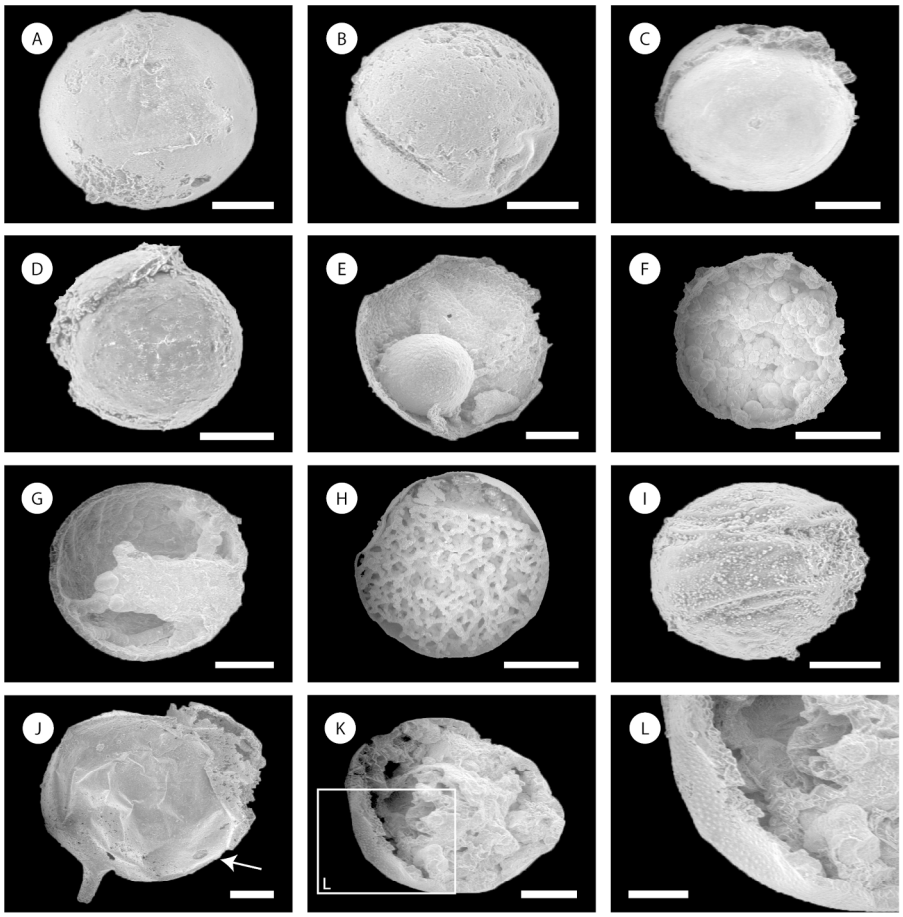

Figure 11. Scanning electron micrographs of *Megasphaera minuscula* (A–J) and *M.* ?*punticulosa* (K–L), acid-extracted from YPM 536747, M618 32.0. A, YPM 538726, may alternatively represent a leiosphere. B, YPM 538727, may alternatively represent a leiosphere. C, YPM 538718, with thick wall. D, YPM 538074, with thick wall. E–H, YPM 538073, YPM 538728, YPM 538729, YPM 538719, all with diagenetic phosphate in the interior. I, YPM 538721, with raised equatorial band. J, YPM 538797, with single large "stalk" and crater (arrow). K–L, YPM 538720, with exterior ornamentation. Scale bars are 50 μm in A, B, D, L; 100 μm in C, E, G, I, J, K; and 200 μm in F, I.

173x232mm (300 x 300 DPI)

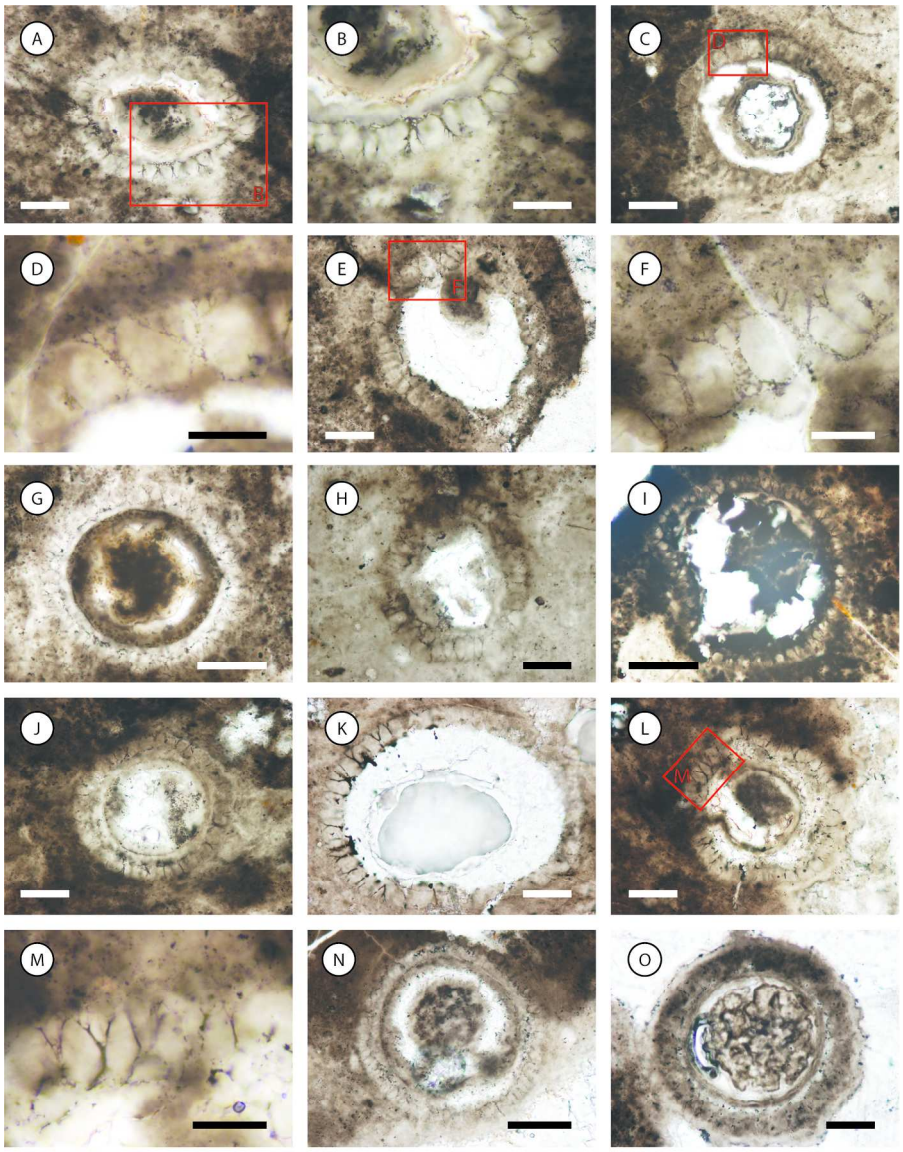

Figure 12. Photomicrographs of *Variomargosphaeridium gracile* in thin-section. A–N, show a diagenetic halo between processes. A–B, YPM 536800, M618 32.0 A, Y61/0, some infilling with silica, internal structure, and feather-like processes. C–D, YPM 536801, M618 32.0 A, K41/2, infilled with silica and internal structure. E–F, YPM 536802, M618 32.0 A, Q69/1, infilled with silica and internal dark area. G, YPM 536803, M618 32.0 A, U51/4, with internal structure. H, YPM 536767, M618 32.0 B, L65/0, infilled with silica. I, YPM 536768, M618 32.0 B, Z40/4, with internal structure and silica replacement. J, YPM 536770, M618 32.0 C, P55/0, infilled with silica and some internal structure. K, YPM 536774, M618 32.0 D, M75/3, infilled with silica. L–M, YPM 536775, M618 32.0 D, O52/4, infilled with silica and some internal structure. N, YPM 536776, M618 32.0 A, B39/0 infilled with silica with some internal structure. O, YPM 536777, M618 32.0 A, U51/4, with diagenetic phosphate infill. Scale bars are 50 µm in A, C, E, G–L, N, and O, 30 µm in B and F; and 20 µm in M.

173x232mm (300 x 300 DPI)

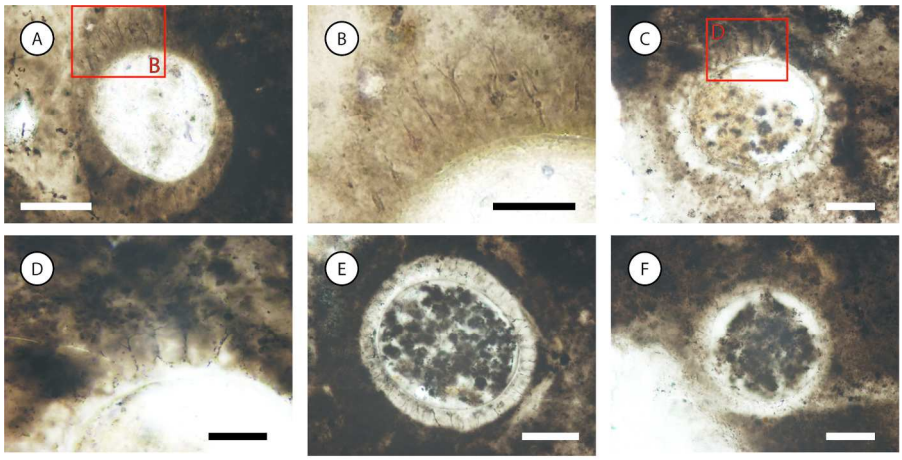

Figure 13. Photomicrographs of further *Variomargosphaeridium gracile* in thin-section. A–B, YPM 536771, M618 32.0 C, F67/1, with slender processes that are long with respect to the vesicle diameter and show evidence of twisting. C–D, YPM 536769, M618 32.0 B, L69/0, with internal cell-like structures (?multicellular). E, YPM 536772, M618 32.0 C, H71/3, with internal cell-like structures (?multicellular). F, YPM 536773 M618 32.0 C, K48/4, with internal cell-like structures (?multicellular). Scale bars are 50 μm in A, C, E, and F; and 30 μm in B and D.

173x232mm (300 x 300 DPI)

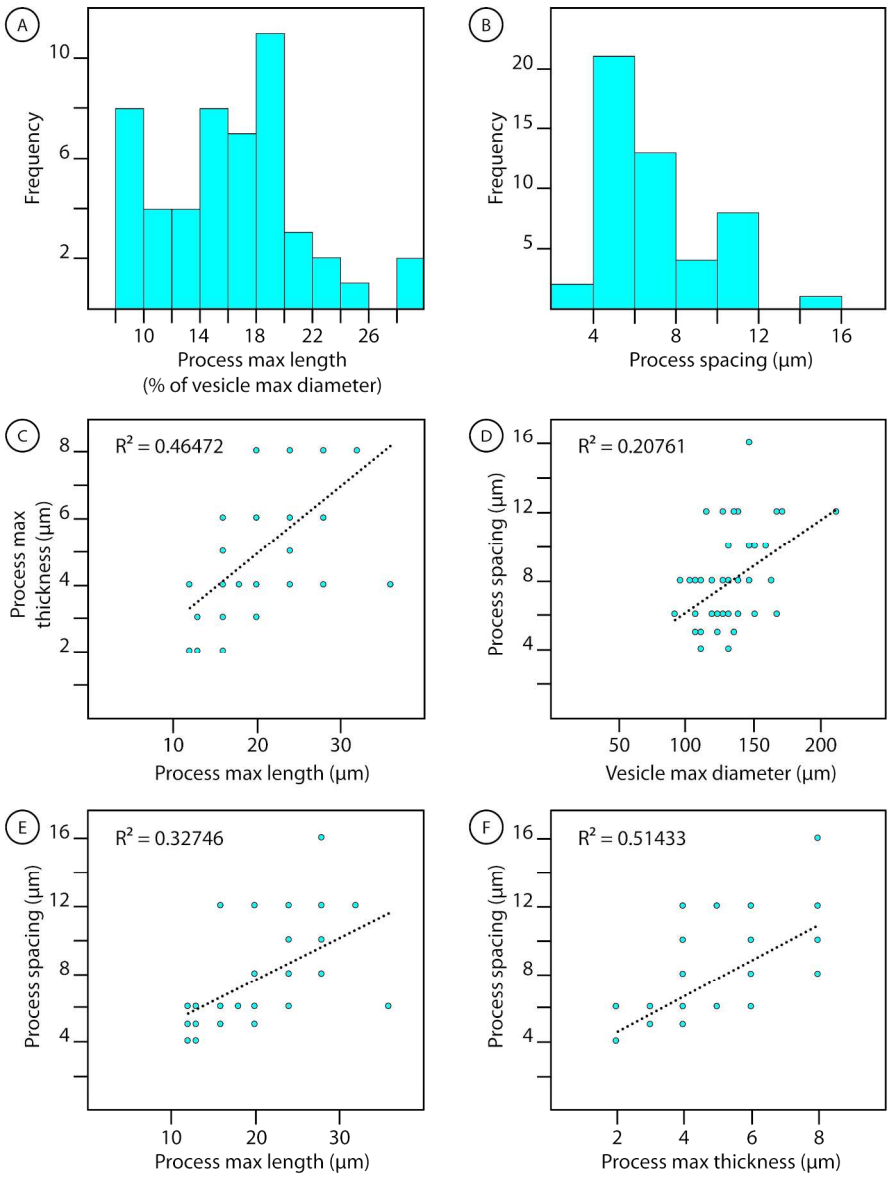

Figure 14. Dimensions of *Variomargosphaeridium gracile*. A, frequency histogram of maximum process length as a percentage of vesicle maximum diameter diameter. B, frequency histogram of process spacing. C, process maximum thickness versus process maximum length. D, process spacing versus vesicle maximum diameter. E, process spacing versus process maximum length. F, process spacing versus process maximum thickness.

173x232mm (300 x 300 DPI)

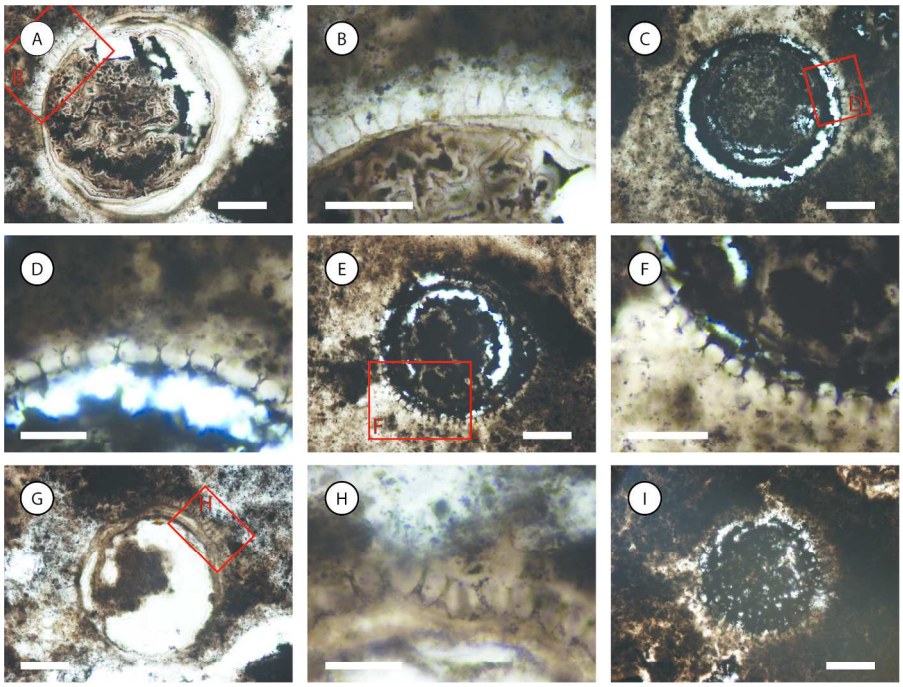

Figure 15. Photomicrographs of *Variomargosphaeridium aculeiparvum* in thin-section. A–B, YPM 536806, M618 33.0 E, Y6/0, with diagenetic phosphate mineralization infilling vesicle interior. C–D, YPM 536786, M618 33.0 A, F58/3, with shrunken interior and silica infill. E–F, YPM 536787, M618 33.0 A, L50/1, with shrunken interior and silica infill. G–H, YPM 536807, M618 33.0 E, P42/3, with silica infill and interior structure. I YPM 536788, M618 33.0 A, E51/4, degraded example. Scale bars are 50 μm in A, C, E, G, and I; 30 μm in B and F; and 20 μm in D and H.

173x232mm (300 x 300 DPI)

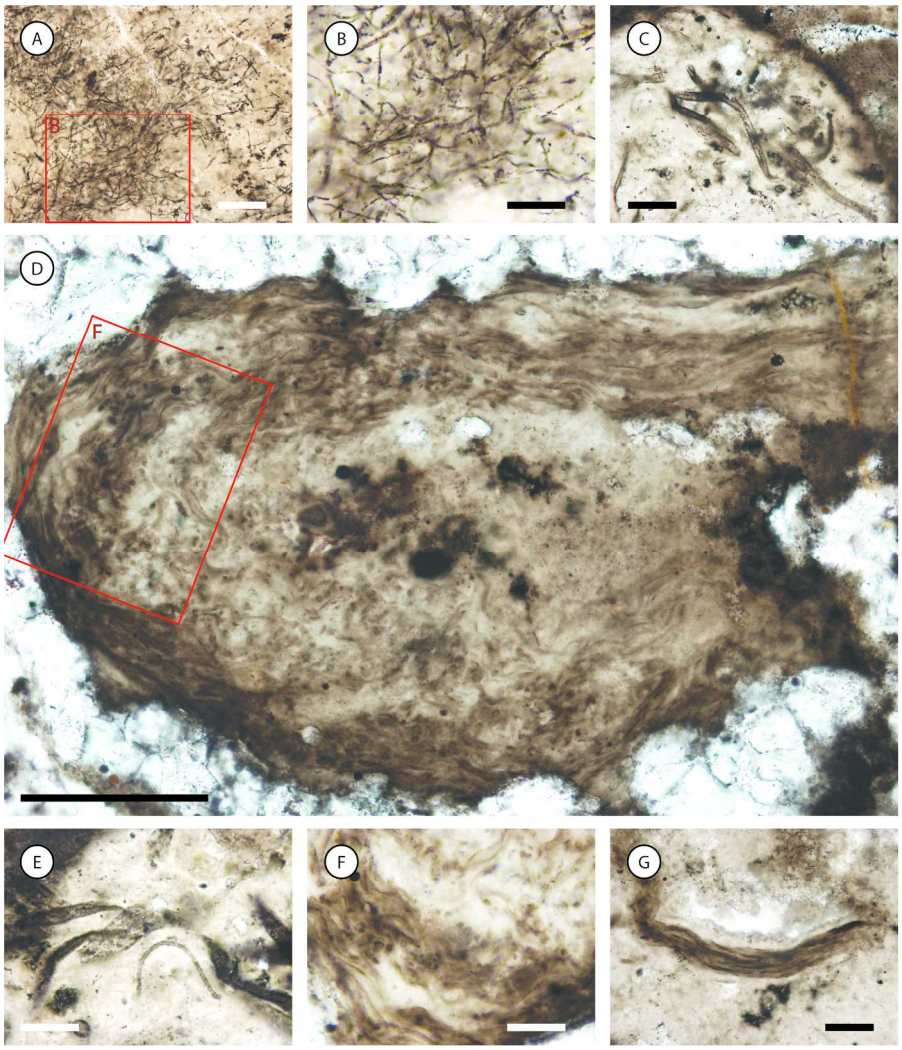

Figure 16. Photomicrographs of *Siphonophycus* in thin-section. A–B, YPM 536789, M618 33.0 A, X53/1, inter-woven criss-crossing mat texture with high concentration of *Siphonophycus* fossils. C, YPM 536797, M618 33.0 C, U53/2, filaments with thickened walls, likely a result of degradation. D, YPM 536808, M618 33.0 F, C54/0, large layered microbial mat clast rounded and folded around itself includes various *Siphonophycus* species. E, YPM 536798, M618 33.0 C, U53/2. F, YPM 536808, M618 33.0 F, C54/0, microbial mat texture from clast in D with *Siphonophycus* filaments. G, YPM 536799, M618 32.0 B, J63/2, small microbial fragment with *Siphonophycus* filaments. Scale bars are 100 μm in D; 50 μm in A, C, and G; and 30 μm in B, E, and F.

173x232mm (300 x 300 DPI)

	Khesen Gol		Urandush Uul	
	YPM 536746 0 m in Fig 2.4	YPM 536749 3 m in Fig 2.4	YPM 536747 21 m in Fig 2.5	YPM 536748 22 m in Fig 2.5
Cyanobacteria				
Obruchevella delicata	R			
Obruchevella magna			R	R
Obruchevella parvissima				R
Obruchevella valdaica				R
?Algae				
Archaeophycus yunnanensis			R	
Acritarchs				
Appendisphaera grandis			R	
Appendisphaera fragilis		R		R
Appendisphaera tenuis			R	
Cavaspina basiconica			R	
Leiosphaeridia crassa			R	
Leiosphaeridia jacutica	R	R	C	C
Leiosphaeridia tenuissima	R	R	C	C
Megasphaera minuscula			C	C
Megasphaera ?puncticulosa			R	
Variomargosphaeridium gracile			C	C
Variomargosphaeridium aculeiparvum				R
Incertae cedis				
Siphonophycus spp.	C	C	C	C